**Master's Thesis of Engineering**

# Application of Electro-Hydraulic Proportional Valve for Steering Improvement of an Autonomous Tractor

전자유압밸브를 이용한 자율 주행 트랙터
조향성능 향상 연구

**August 2017**

**Graduate School of Agriculture and Life Sciences**
**Seoul National University**
**Major of Biosystems Engineering**

**CHANGJOO LEE**

# Application of Electro-Hydraulic Proportional Valve for Steering Improvement of an Autonomous Tractor

## Professor HAKJIN KIM

## Submitting a master's thesis of Engineering

## August 2017

## Graduate School of Agriculture and Life Sciences
## Seoul National University
## Major of Biosystems Engineering

## CHANGJOO LEE

## Confirming the master's thesis written by
## CHANGJOO LEE
## August 2017

Chair       <u>Seong-In Cho</u> (Seal)

Vice Chair <u>Hak-Jin Kim</u> (Seal)

Examiner    <u>Jung-Hun Kim</u> (Seal)

# Abstract

The most common solution to achieving automated steering in an agricultural tractor is the use of an electric motor in parallel with a conventional hydrostatic valve-based hydraulic steering system owing to its simplicity and low cost. However, the existing overlap, or dead band, of a hydrostatic valve has limited its potential benefit to automated tractor steering in terms of providing various agricultural operations, including planting and spraying, at higher speeds. The main objective of this study was to develop an electro hydraulic steering system applicable to an auto-guidance system, and to compare the performance of the developed system with a conventional automatic steering system. A proportional-feedforward control algorithm was implemented to effectively compensate the non-linear behaviors of the hydraulic cylinders used for changing the steered wheel angle of the tractor. A computer-controlled hardware-in-the-loop electro-hydraulic steering simulator consisting of two different types of valve sub-systems s, i.e., hydrostatic valve and EHPV sub-system, was designed and built for the development of the steering control algorithms and to verify the feasibility of the developed steering controller for accurate steering of the system with acceptable response times. A field test was conducted using a Real Time Kinematic GPS based autonomous tractor equipped with the developed EHPV-based steering system and an EPS-based steering system used as a control to compare and investigate their potential in enhancing the path tracking functionality of an auto-guided system. The use of the EHPV-based steering controller was shown to improve the tracking error by about 29% and 50% for straight and curved paths, respectively, as compared to the EPS-based steering system.

**Keyword :** Autonomous tractor, Electro-hydraulic steering valve, Hydrostatic valve, Hardware-in-the-loop simulator, Nonlinear.

**Student Number :** 2015-23023

# Table of Contents

# List of Tables

# List of Figures

# Nomenclature

$A_n$      flow section area (mm$^2$)

$A_{pv}$      orifice area of the load control valve (m$^2$)

$A_p$      cylinder area of the load cylinder (m$^2$)

$c(s)$      curvature of path C at that point (m$^{-1}$)

C      path to be followed

$C_d$      valve orifice coefficient

d      impulse duration (ms)

$d_h$      hydraulic diameter (mm)

$f_P(u)$      nonlinear gain function of the E/H steering system

$G_P(s)$      open-loop transfer function

$G_l(s)$      linear transfer function

I      impulse amplitude

$k_1$, $k_2$      constant values

L      vehicle wheelbase (m)

M      point on C which is the closest to O

O      center of the vehicle virtual rear wheel

ΔP      pressure drop across an orifice (N/m$^2$)

$q_i$      input (target angle, $\theta_r$) variable of physical system (°)

$q_o$      output (steered wheel angle, $\theta_y$) variable of physical (°) system (°)

Q      flow rate (L/min)

$Q_i$, $Q_o$      Laplace transform of the time functions $q_i$ and $q_o$

$Q_p$      flow rate across the load control valve (m$^3$/s)

$R_x(n)$, $R_y(n)$     reference path (m)

P         pressure in both chambers of the steering cylinder (Pa)

s         curvilinear abscissa of point **M** along **C**

$t_0$        time when the threshold value is exceeded (s)

v         tractor linear velocity at point **O** (m/s)

$v$        average flow velocity (m/s)

V         piston speed (m/s)

$x_c$, $y_c$    center of turning path (m)

$x_g$, $y_g$    current tractor position (m)

y         lateral deviation of the tractor with respect to **C** (m)

$\dot{y}$        velocity of steering actuator (m/s)

λ         viscosity-temperature coefficient

$\eta$        dynamic viscosity at reference temperature θ (℃) (kg/m·s)

$\eta_0$       dynamic viscosity at reference temperature θ₀ (℃) (kg/m·s)

$\widetilde{\theta}$        angular deviation of the vehicle (°)

$\theta_c(s)$     orientation of the tangent to **C** at that point (°)

$\theta_t$        orientation of the tractor centerline (°)

$\tau_{DT}$,     dead-time value (ms)

δ         orientation of the front wheel with respect to tractor centerline (°)

ρ         fluid mass density (kg/m³)

# Chapter 1. Introduction

## 1.1.    Study Background

Most agricultural field operations are performed using parallel swathing or switchback operation. Each subsequent pass across the field should be parallel to the previous and separated by a distance equal to the treatment width of the implement. This kind of operation is very repetitive and can become monotonous for the operator (Stombaugh, T., 1997).

Automatic steering technology is a revolutionary invention in agricultural machinery that completely changed the way farm. This technology is currently being used very effectively for planting, spraying, and harvesting of row crops. It can lower costs and increase profits by improving efficiency and productivity of farm operations. Auto-guidance systems have the capability to steer a vehicle across the field in a straight line or any predetermined track (Ehsani. R., and E. Ontermaa, 2011).

In agriculture, accurate vehicle steering is an important objective. Auto-guidance systems can potentially steer a vehicle more precisely than can a human operator, such as tilling, planting, spraying, fertilizing, harvesting and other farming operations.

Tractor implements are guided through accurately-spaced passes or swaths, the spacing of which is determined by the swath width of the equipment. However, gaps and overlaps can occur when operators deviate from the ideal guide paths, resulting in under-coverage and over coverage respectively. Such gaps and overlaps are detrimental to agricultural operations and can reduce crop yields. For example, gaps in coverage reduce the effective areas of yields being cultivated and treated. Overall crop production may suffer as a result. Overlaps in coverage tend to be inefficient and wasteful of materials, such as fertilizer, pesticides, herbicides, seed, etc. Another potential problem with overlapping coverage relates to the potential crop-damaging effects of double applications of certain agricultural chemicals.

Conventional steering system used in construction and agricultural machines alike is a so-called hydrostatic steering system. The vehicles have traditionally utilized a full fluid-linked steering system in which turning the steering wheel rotates the hydrostatic valve which is mechanically coupled to the steering shaft and opens a control port which releases flow of hydraulic fluid to the steering cylinder.

The most common solution to active steering for auto-guidance systems is a combination of an electric motor in parallel with the

hydraulic system, which is a simple, less expensive and easily installed the steering system that minimizes or eliminates substantial steering system modifications (Amico, A. D., 2016). The present invention shown in Fig. 1 relates to automatic steering systems for vehicles. Nelson et al (2006) developed structure for converting a conventional steering system of an off-road vehicle to automatic steering system.



Fig. 3
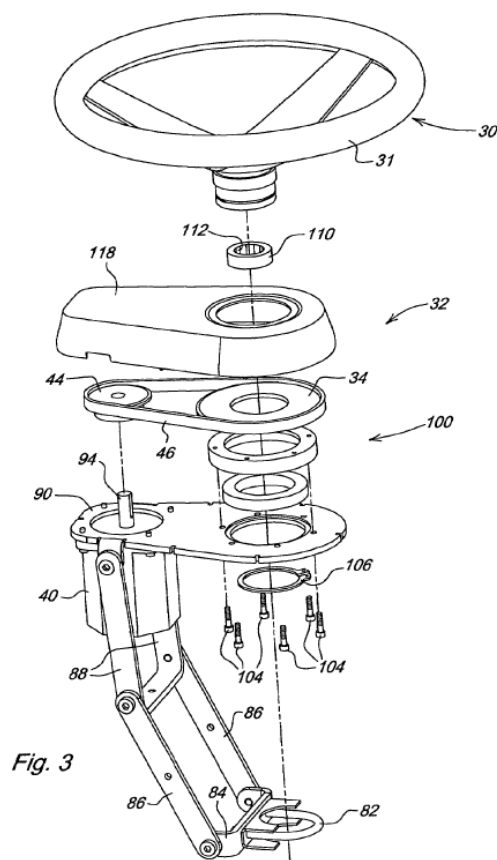
**Fig. 1 Automatic Steering System (U. S. Patent 7,349,779 B2). A motor 40 mounted on the end of the steering shaft 20 to provide direct drive to the shaft 20 at a location offset from hand grip portion 30.**

However, such a motor-based steering system has some disadvantages. First, on account of the necessarily existing overlap of the hydrostatic valve for a control port, hydrostatic steering has a relatively high steering play of up to $\pm 5°$. Further, there is a dead time between the start of steering wheel movement and the steering cylinder movement. Second, the design is relatively elaborate because, on account of the relatively long distance between the steering wheel, steering shaft and the axle where the steering cylinder is located, correspondingly long hydraulic pipes have to be installed. This, when added to the amount of the above-mentioned steering play, creates a dynamic behavior which is difficult to influence given the nature of the hydraulic circuitry and the hydraulic components used. Optimization can be obtained only with difficulty by adjustment of the hydraulic components. The dynamic behavior is such that it is difficult to drive exactly straight ahead, which at relatively high traveling speeds places high demands on control abilities (Diekhans, 2000).

Since the purpose of this study is to improve the performance of conventional steering systems, a possible solution would be to use electro-hydraulic proportional valve (EHPV). These are actuated by a solenoid, thereby providing an electronic interface. An

electrohydraulic solution takes advantage of the high power density

from fluid power systems, which gives a very compact solution

(Amico, A. D., 2016).

## 1.2. Description of Tractor Steering System

The power required when steering a tractor is very high compared to a passenger car. This becomes obvious when considering the relative difference in front axle load. The tractors have traditionally utilized a full fluid-linked steering system, and the most common front axle steering arrangement for a hydraulic steering cylinder. Because of their high power density in comparison to its volume, hydraulic drives are qualified for the use in vehicles with high steering loads.

The different parts of a conventionally steered front axle on a tractor are shown in Fig. 2. The steering hydrostatic valve shown in Fig. 3 is connected to the steering wheel and to both ends of the piston-and-cylinder steering unit by hydraulic lines. The hydrostatic valve, usually of the rotor type, performs both the operation of supplying the operating fluid to the power cylinders for steering the wheels and the metering of the fluid required to perform the steering operation. This type of hydraulic steering system is satisfactory for conventional tractors, trucks and earth moving equipment.
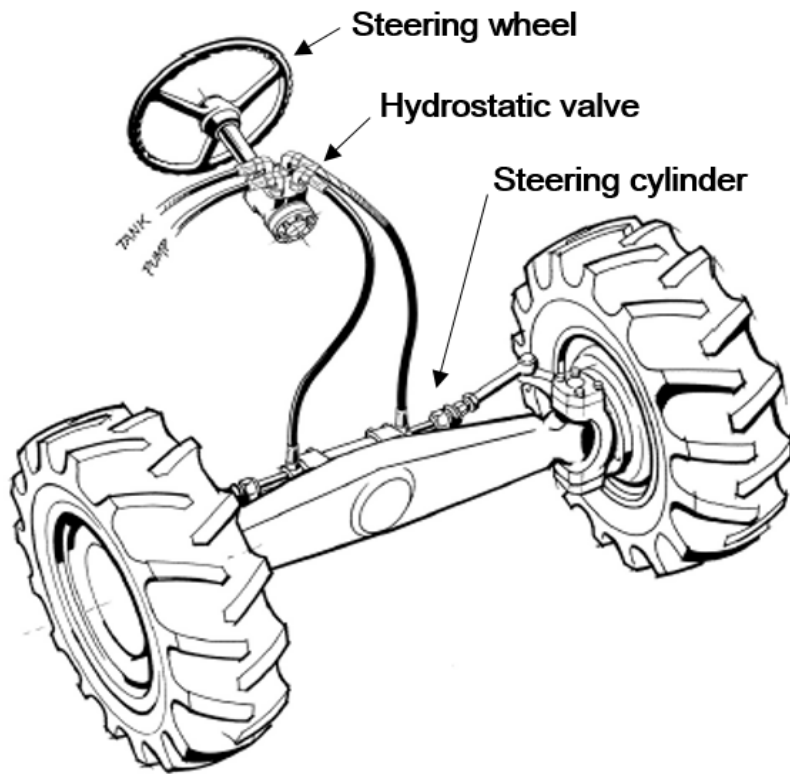
**Fig. 2 Conventional steering system (Source: Danfoss).**



**Fig. 3 Hydrostatic steering valve (Source: Danfoss).**

In hydraulic steering systems for land vehicles, the most commonly used form of valve for use in power-assisted steering mechanisms is a hydrostatic valve. The hydrostatic valve includes a valve arrangement including a spool that extends through a sleeve. The spool and the sleeve are coaxially aligned along an axis, and a limited range of relative rotational movement about the axis is permitted between the spool and the sleeve. The valve arrangement is normally biased toward a neutral state. The valve arrangement is displaced from the neutral state to an operating state by rotation of a steering wheel coupled to the spool. When the valve arrangement is in the operating state, pressurized fluid flows through the valve arrangement and into a fluid pressure actuated a rotor, thereby releasing the flow of hydraulic fluid to the steering cylinder.

Each lobe of the rotor has a diametrically opposite lobe, when one lobe is in a cavity its opposite lobe is at the crest of the stator's convex form opposite the cavity (Fig. 4). As the rotor is rotated, each lobe in sequence is moved out of its cavity to the crest of stator's convex form and this forces each opposite lobe, in sequence, into a cavity.
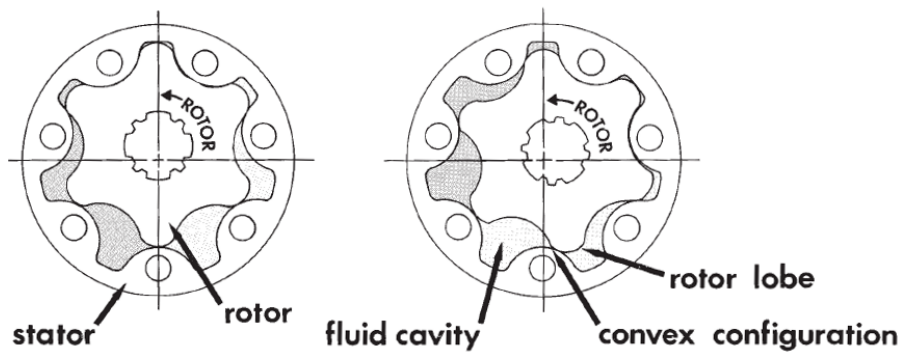
**Fig. 4 Rotor operation in the rotor set (Source: Parker Hydraulics)**

Operating state means a state where sufficient pressurized flow passes through the valve arrangement to drive movement of the rotor displacement mechanism. There has generally been excessive "neutral dead band" because of steering wheel can reverse direction with little or no resistance. When relative rotation is first generated between the spool valve and the valve sleeve, the valve arrangement initially passes through the dead band, typically $\pm 5°$ degree or so, where insufficient flow passes through the valve arrangement to drive the displacement mechanism. Once the valve arrangement rotates past the dead zone, the valve arrangement is in the operating state where sufficient flow passes through the valve arrangement to drive movement. However, such that the steering control at relatively higher vehicles speeds is unacceptable because there is a time delay between the start of steering wheel movement and the steering cylinder movement.

## 1.3.  Automatic Steering System

### 1.3.1.  Electric Power Steering System

A change of hydraulic systems to solely electrically operated steering systems (Electric Power Steering, EPS) has taken place in passenger car steering systems during the last years. The use of these systems was originally limited to small vehicles because the power density of the electronic parts and the energy available from the on-board wiring was not sufficient to serve bigger vehicles and higher steering powers (Harrer, M., and P. Pfeffer. 2015).

Active steering is referred to as the possibility to control the output torque required to turn the wheels or manipulate the steering angle with an electronic signal. The most common solution to active steering for tractors is a combination of an electric motor and the hydraulic system. There are universal steering systems available as retrofit solutions. In this case, an electric motor is either frictionally or force-fit engaged to the steering column. There is no direct interaction with steering hydraulics. Examples of those retrofit solutions are John Deere Auto Trac Universal, Topcon electric steering system and Trimble EZ-steer (Winner, H., S. Hakuli, F. Lotz and C. Singer, 2015, Fig. 5, 6).

**Fig. 5 Photograph of Topcon electric steering system**



**Fig. 6 John Deere Auto Trac Universal**

## 1.3.2. Electro Hydraulic Steering System

Electro-hydraulic (E/H) steering systems are being developed for heavy-duty industrial machines because of their potential versatility over mechanical and hydraulic steering systems. Its relatively high power-to-weight ratio and electronic controls provide effective means of power transmission. However, including load dependent dead-band, asymmetric flow gain, hysteresis, saturation, and time delay, results in difficulties in designing high performance steering systems.

A basic system consists of a pilot steering unit as the signal source and an electro hydraulic steering valve block which controls oil flow to the steering cylinders proportional to the pilot flow. The system can be extended to include an electrical actuator so that, as an alternative, it becomes possible to steer with a joystick
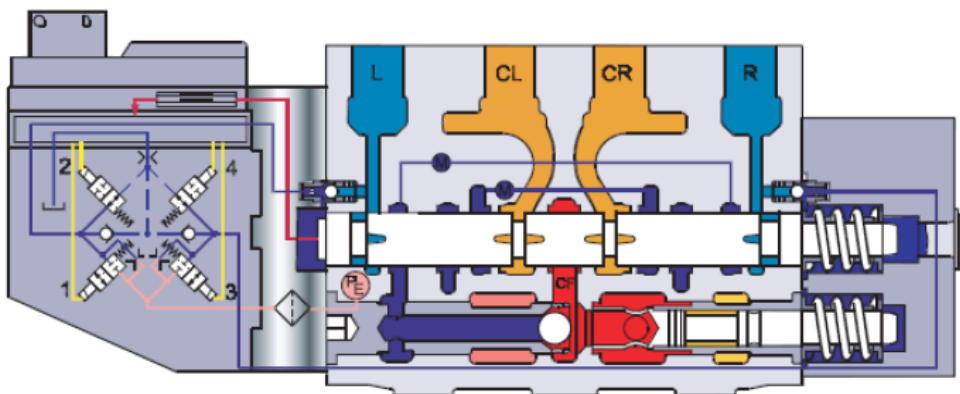


**Fig. 7 Electro hydraulic steering valve with electrical actuation unit (Source: Danfoss).**

## 1.4. Review of Literature

**Electro-Hydraulic Steering Controller**

Zhang et al. (2000) designed an E/H steering system for off-road vehicles. Their E/H system exhibits nonlinear behaviors, limiting the use of computer simulations to investigate its system dynamics. A hardware-in-the-loop (HIL) E/H steering simulator was developed to improve the efficiency in researching the E/H steering dynamics. With an appropriate orifice opening control, the simulator is able to simulate the desired load applied to the system.

E/H systems are highly non-linear with a large dead band, non-linear flow gain, and saturation. Conventional control technologies such as a proportional-integral-derivate (PID) controller have limitations in providing satisfactory steering control for off-road vehicles. Qiu et al. (2001) designed an FPID controller to provide satisfactory steering control. Their FPID controller consists of a feedforward loop and a PID loop. The feedforward loop was designed to compensate for the dead band and saturation inherent to an E/H steering system, and an inverse valve transform was adopted to determine the appropriate degree of valve opening. Furthermore, to overcome the static friction, an impulse excitation signal generator was used.

13

Zhang. (2003) developed a generic fuzzy controller applicable to a hydraulic cylinder owing to its ability to compensate for non-linearity of the system. A hierarchical control rule derivative technique was developed to create the control rules for the generic controller.

Jiang. (2009) developed a PID-based steering controller using an E/H valve. Through step-response tests, the PID-based algorithm was shown to work well under different external load forces. However, the flow rate affects the control precision of the steering controller, and a corresponding PID value is used to accurately control the cylinder position. An additional model is needed to compensate for the flow rate.

Lenain et al. (2006) designed a model prediction control for compensate actuator delays, which is adapted to the control law with incorporated sliding control and enables both anticipation of an approaching curvature and sliding compensation. The reference path geometry and low-level model enable the anticipation of an approaching curvature. Using such information, it is possible to send a control value to the actuator the moment before a curve appears.

Rekow et al (2007) developed a stable steering control system, which includes a hydrostatic valve coupled to the steering wheel for

14

generating a hydraulic signal as a function of the steering wheel positioning, an electro-hydraulic valve that generates a hydraulic signal that functions as an electronic control signal, an electronic control unit an generating the electronic control signal, and a hydraulic unit combining the first and second hydraulic signals and supplying a hydraulic control signal to the hydraulic steering actuator. As shown in Fig. 8, a T unit (16) combines the flows from the valves (14) and (18), and supplies the combined flow to a conventional steering cylinder (20) (Fig. 8). The benefit of this system is that it naturally compensates for a dead band or hysteresis occurring in the hydro-mechanical parts of the system. The system continuously monitors and augments the stability of the vehicle.



Fig. 1
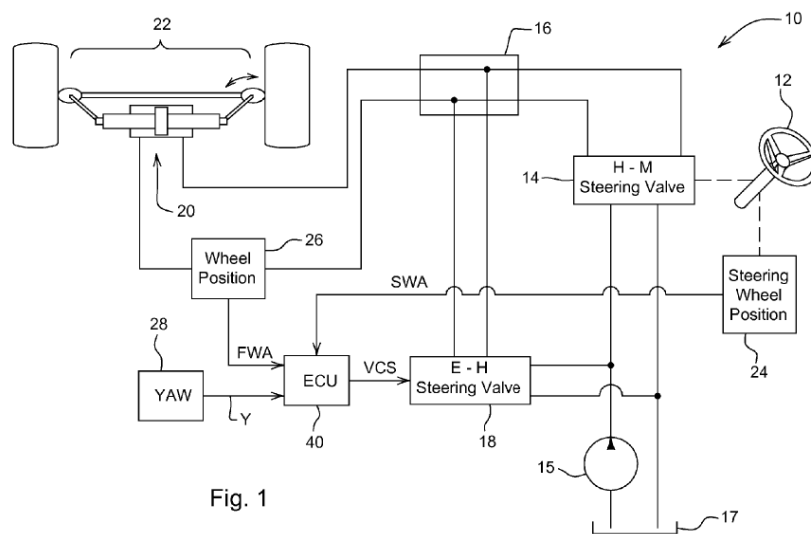
**Fig. 8 Schematic diagram of the steering control system (U. S. Patent 0256884 A1).**

15

## 1.5.　　Research Purpose

Little research has been reported on the performance differences between motor and spool-based steering systems. It is not clear what issues are critical to a conventional steering system. Therefore, the main objective of this study was to develop an electro hydraulic steering system capable of being used in an auto-guidance system, and to compare the performance of the developed system with a conventional automatic steering system.

The specific sub-objectives of this study are as follows:

1. Develop an HIL steering simulator for easier problem detection, and encourage the development of a new steering system.

2. Analyze of the response capabilities and dynamic characteristics of the hydrostatic valve.

3. Design an electro-hydraulic steering controller capable of providing automatic steering in an agricultural vehicle.

4. Compare the performance of the steering controller with a conventional steering system under actal field conditions.

# Chapter 2. Materials and Methods

## 2.1. Preliminary Performance Test of Conventional Steering System

### 2.1.1. Purpose of Preliminary Test

Before starting the design of the simulator, preliminary vehicle tests were conducted to evaluate the performance of a conventional steering system and to find directions for improvement. In addition, to determine the range of load to apply to the laboratory-scaled simulator, it was necessary to evaluate not only the steered wheel characteristics but also the steering loads on an actual tractor.

A photograph of the experiment system used in this study, a TongYang Moolsan Model TX803 tractor, is shown in Fig. 9. The tractor used an open-center hydraulic circuit equipped with a hydrostatic steering valve. A fixed displacement gear pump driven by an engine was used to supply a constant flow to the hydrostatic valve.

An EPS (Unmanned Solution) was used in the steering column to rotate the steering wheel, and was controlled through CAN communication. Based on the target angle determined by the EPS control module, the current from the motor drive circuit to the EPS motor was controlled to within the target amount, and the motor operated accordingly. The front wheel angle was measured using a

rotary encoder, and the sensing shaft was attached to a king pin of the wheel being monitored (Fig. 10). In addition, pressure sensors were used to measure the chamber pressure conditions and calculate the loading forces (Han, X. Z., 2013, 2017).

**Fig. 9 System configuration of the test tractor.**

**(TongYang Moolsan Model TX803 tractor)**



**Fig. 10 Steering angle sensor mounting position.**

**Table 1 Specifications of the test tractor**

| Name | Specifications |
|------|----------------|
| Gear pump | − Displacement : 9.0 cc/rev<br>− Speed ratings : 500 ~ 3000 RPM<br>− Max pressure : 210 kgf/cm$^2$ |
| Hydrostatic Steering valve | − Rated Flow : 16 LPM<br>− Displacement : 120 cc/rev<br>− Relief valve pressure : 145 ~ 150 kgf/cm$^2$<br>− Open center<br>− Non load reaction type |
| Hydraulic steering cylinder | − Cylinder stroke : 123mm<br>− Piston diameter: 60Φ<br>− Rod diameter: 35 Φ<br>− Working pressure : 100kgf/cm2<br>− Double acting<br>− Double rod |
| EPS | − Continuous torque : 0.52 N-m<br>− Peak torque : 0.84 N-m<br>− Nominal continuous power : 204 Watt<br>− No load Speed : 5,200 RPM<br>− Rotor inertia : 0.706 10$^{-5}$kg-m$^2$ |
| Steer sensor | − Model :ComeSys RD06001<br>− Steer sensor travel : 360 deg<br>− Analogue output |
| Pressure sensor | − Model : HySense PR 110<br>− Range : 0 ~ 600 bar<br>− Signal : 0 ~ 20 mA |

### 2.1.2.  Zero-Load Test

The forces and moments exerted on turning wheels originate from the ground's reaction to the steering action generated at the tire-ground interface (Mas, F. R., and Z. Qin, and A. C. H., 2010).

To investigate the steered wheel characteristics in response to an applied load, steering response experiments were carried out under no load conditions, with a flow rate of around 10.5 LPM. (Zhang. Q., J. F. Reid, and D. Wu, 2000).

As shown in Fig. 11, the front wheel axle of the tractor was raised from the ground.

The EPS provided step input commands through the steering wheel, and the steered wheel angle and chamber pressures were measured at 50 Hz.



**Fig. 11 A zero-load test to investigate the steering characteristics of the EPS-based steering system.**

### 2.1.3. Tractor Traveling Test

To obtain data on the steering characteristics under an actual traveling environment, the steering response experiments were performed at constant speeds on a farm. Fig. 12 shows test location on the Seoul National University Farm in Suwon. Fig. 13 and Table 2 represents the physical properties of the soil and soil characteristics were classified as Sandy Loam according to USDA (Han, X. Z., 2017).



**Fig. 12 Test fields in Suwon**

**Fig. 13 Soil sampling areas.**


**Table 2 Soil properties and moisture contents of test fields.**

|  | Items | Values |
|---|---|---|
| **Section A** | **Sand (%)** | **36.88** |
|  | **Silt (%)** | **38.68** |
|  | **Clay (%)** | **24.44** |
|  | **Moisture content (%)** | **22.8** |
| **Section B** | **Sand (%)** | **34.96** |
|  | **Silt (%)** | **39.04** |
|  | **Clay (%)** | **26.00** |
|  | **Moisture content (%)** | **19.41** |

## 2.2. Hardware-in-the Loop Simulator

Hardware-in-the-loop is the simulation technique where a part of the software implemented simulation model is replaced by actual hardware. This has the advantage of being able to test parts of the system without going for the full prototype, especially for large systems (Amico, A. D, 2016).

It is difficult to evaluate steering system properly such as steering response characteristics without actual vehicle test. But if steering system can be evaluated more accurately during the simulator which is carried out before actual vehicle testing, it will be possible to detect problems more easily and to encourage the development of a new steering system.

This section 2.2 gives an overview of the hardware involved in the HIL simulator.

### 2.2.1. Hydraulic Circuit

A schematic view of the steering system of a circuit is shown in Fig. 14. In this study, the conventional system is not be tampered with so that manual capability is not lost, and the electro-hydraulic steering capability to the tractor is added for system comparison.

The simulator was basically build up a full fluid-linked steering system and used the conventional open-center circuit. The hydraulic circuit has manual and automatic steering modes for selectively steering steerable wheels of the vehicle. In the manual mode, the flow is directed only toward the hydrostatic valve. When an EHPV is controlling a spool in the manual mode, a steering cylinder cannot be operated. On the other hand, in the automatic steering mode, when a directional valve is powered on, the flow passes through the EHPV and the hydrostatic valve. The directional valve is 2-way normally open solenoid directional valve from HYDAC. A loader system is designed a closed-circuit, and a detail description of a loader system follows below.
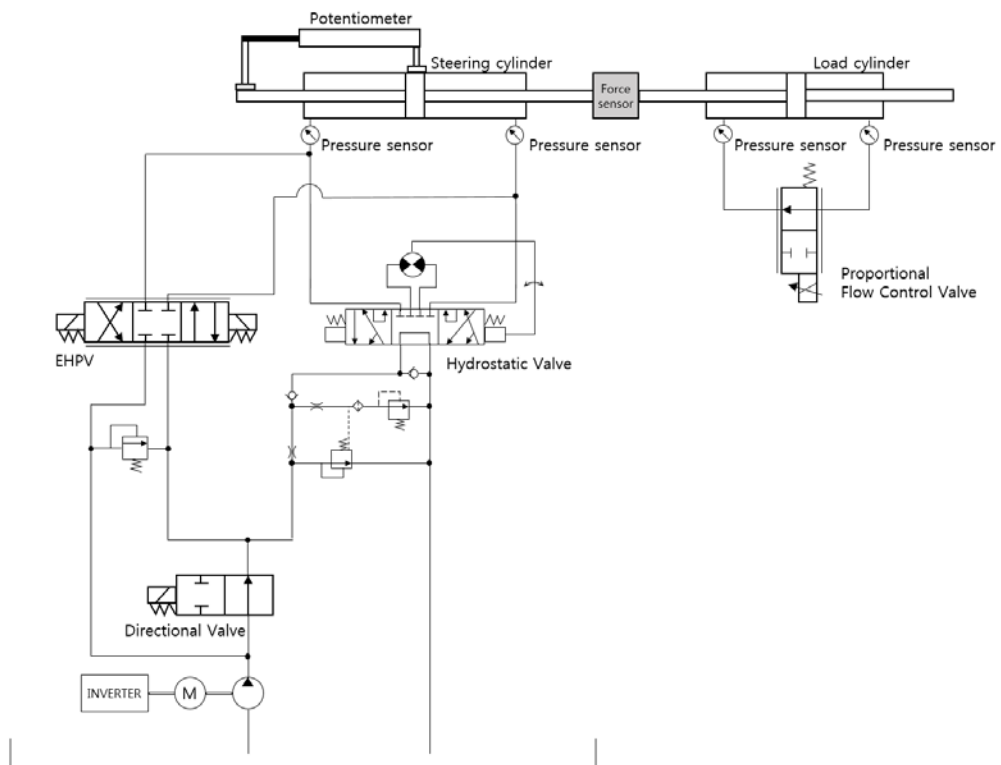
**Fig. 14 Schematic view of steering system of the circuit.**

### 2.2.2. Hardware Description

A photograph of the HIL simulator is shown in Fig. 15. As shown in Fig. 16, actuators of this HIL simulator consists of a steering cylinder and a load cylinder, which is connected in series.

The steering cylinder get their power from pressurized hydraulic fluid by the hydrostatic valve and the 4/3 EHPV respectively.

An EPS is connected through gears on the steering shaft to control the hydrostatic valve and connected to a microprocessor which is controlled via CAN communication and moves with the steering shaft. The EHPV is a hydraulic electrically controlled servo valve, PVG 32 model, from Danfoss. The EHPV built in a PVED-CC that is a digital controlled actuator for PVG 32, which is compliant to the ISOBUS standard for flow control. Fig. 17 shows spool characteristic curves of a PVED-CC, configurable range 1(linear) to 16. In this study, linear curve, default value 1, was chosen. The spool is controlled by flow commands in steps of 0.4% or by spool position with 250 positions.

A fixed displacement gear pump driven by an electric motor, which produces a maximum flow of 24.5 liters per minute, is used in the hydraulic system (Fig. 18). An AC motor inverter, iG5A model from LSIS, varied the angular speeds of the motor shaft.
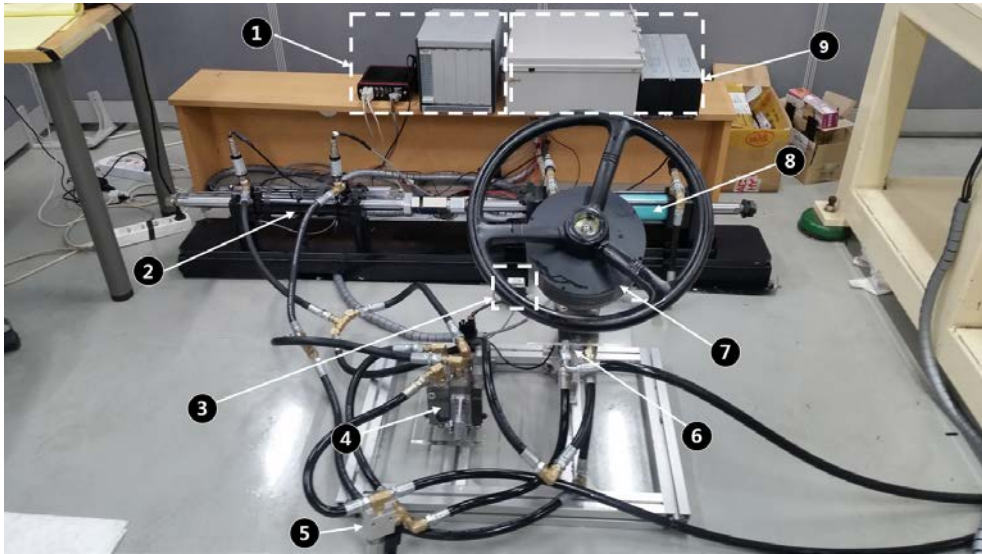
**Fig. 15 Photograph of the HIL simulator (①: Controller & Data acquisition units, ②: Steering cylinder, ③: Proportional flow control valve, ④: EHPV, ⑤ : Directional valve, ⑥: Hydrostatic valve, ⑦: EPS, ⑧: Load cylinder, ⑨: Power supply units)**
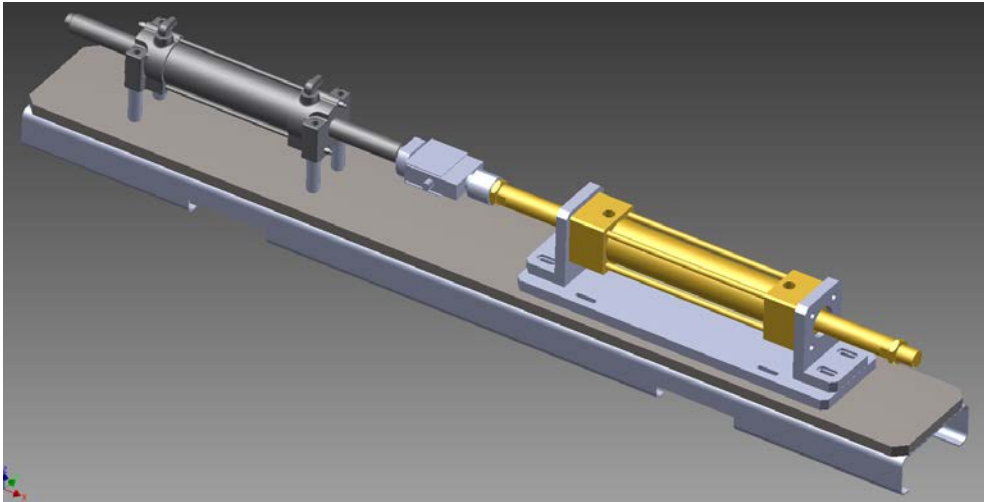


**Fig. 16 HIL simulator 3D CAD model.**
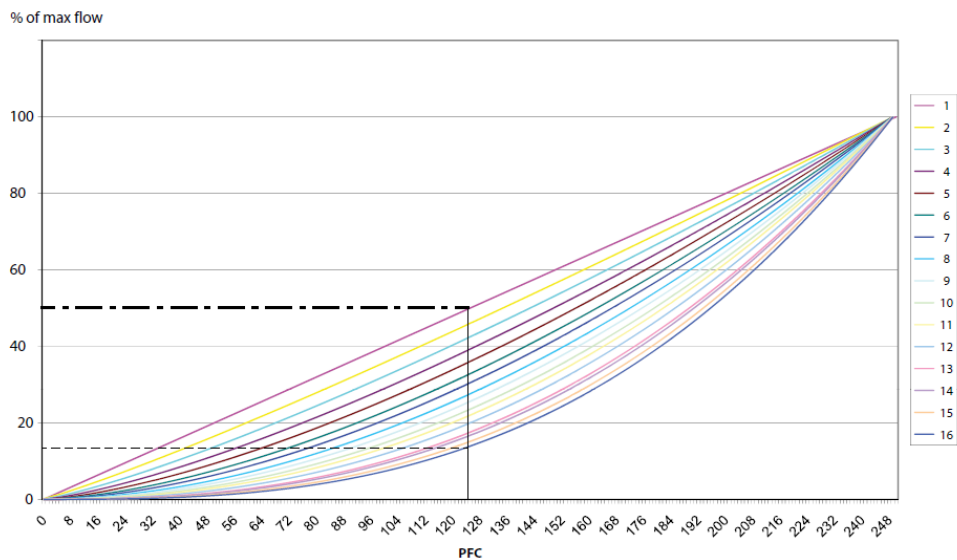
**Fig. 17 Spool characteristic curves. Slope curve is a progressivity scaling of the set point.**



**Fig. 18 Gear pump.**

A photograph of a location of sensors in the HIL simulator is shown in Fig. 19, and Table 3 shows specifications of sensors used in HIL simulator. To measure the steered wheel angle, a potentiometer is fitted on the steering cylinder. Since the steered wheel angle and the cylinder displacement has a direct relationship, the steered wheel angle values are calculated by measuring the cylinder stroke. Fig. 20 shows the relationship between cylinder displacements and steered wheel angles, which is obtained using the TX803 tractor.

Pressure sensors are used to measure the pressure each cylinder both chamber pressures, and pump pressures, and a force sensor measures the force applied by the load cylinder.
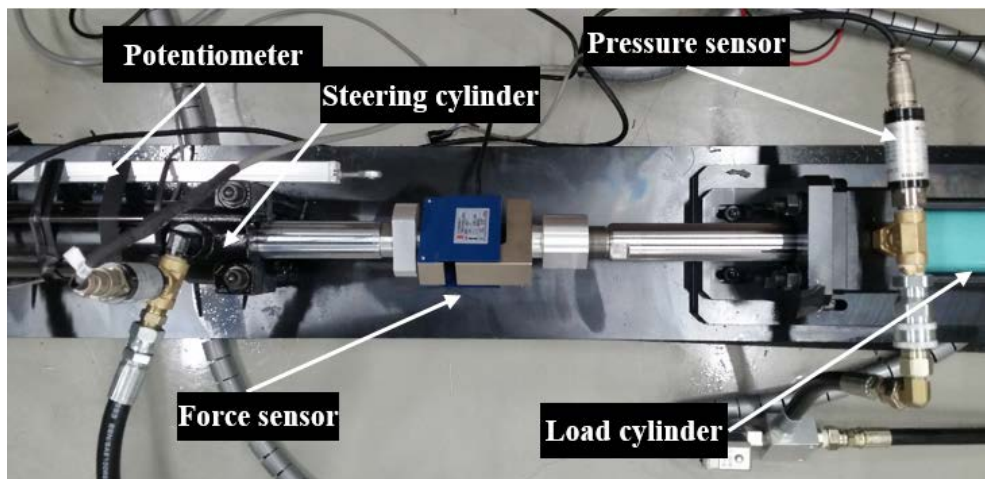


**Fig. 19 Location of sensors in the HIL simulator**

**Table 3 Specifications of sensors**

| Name | Specifications |
|---|---|
| Potentiometer | − Manufacturer : MINOR<br>− Model :KDC<br>− Range : 0 ~ 300mm |
| Pressure sensor | − Manufacturer : VALCOM<br>− Model : VKRQ<br>− Range : 0 ~ 35 Mpa<br>− Strain gage type |
| Force sensor | − Manufacturer : Curiotec<br>− Model : CSB-1T<br>− Capacity : 1tf |
| Flow sensor | − Manufacturer : HYDROTECHNIK<br>− Model : HySense QG<br>− Range : 0.05 ~ 3000 LPM<br>− Gearwheel type |
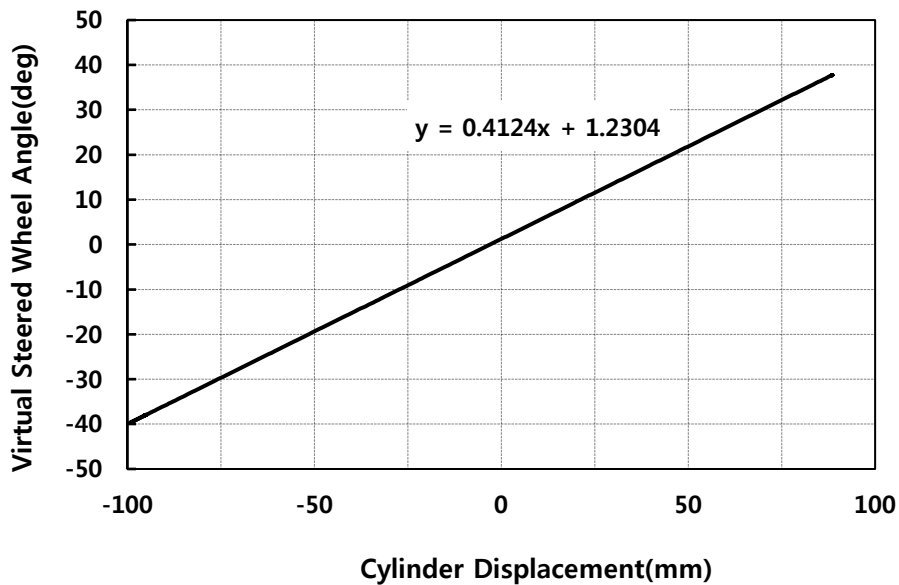


Fig. 20 Cylinder stroke versus virtual steered wheel angle.

The EHPV is controlled by an embedded real-time processing hardware, VN8910A with inserted VN8950 CAN module from Vector (Fig. 21). Fig. 22 shows an I/O interface module (VT2816, Vector) that provides 12 inputs and 4 outputs for analog signals. They may be connected directly to the inputs or outputs of an ECU. The embedded real-time processing hardware runs on CANoe software and can be operated in a stand-alone mode, allowing the system operation without any additional user PC.



**Fig. 21 The embedded real-time processing hardware.**

CANoe software was developed to meet the essential needs of the CAN-based module or system developer by combining a comprehensive set of measurement and simulation capabilities. CANoe can interface to multiple CAN networks (or other common small area network protocols), and provide accurate time-stamped

measurements for all communication transfers. Fig. 23 shows power supply units that convert AC power from the wall into the right kind of power for the individual parts.



**Fig. 22 I/O interface module.**
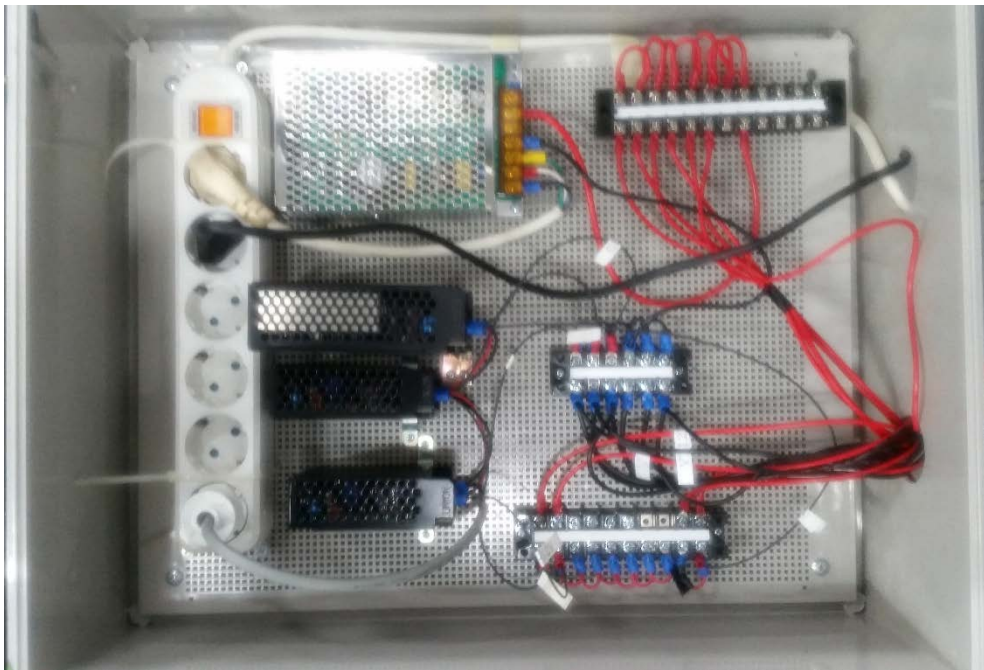


**Fig. 23 Power supply units.**

The loader system is designed to provide loads on the steering cylinder. The load cylinder is attached to generate the load experienced by the steering system, and this system consists of a double rod, double-acting hydraulic cylinder, and a proportional flow control valve (Fig. 24). The proportional flow control valve is a normally closed, direct-acting, spring-loaded, spool type proportional flow control valve, PWK06020V model, from HYDAC.

Between the load cylinder and the steering cylinder, the force sensor measures the force applied by the load cylinder. The loader system is designed a closed-circuit flow to allow fluid movement between the chambers due to the load (Fig. 25). The load on the steering cylinder is determined by the pressure drop across the piston of the load cylinder which is controlled by the orifice area of the proportional flow control valve and the speed of the piston. The orifice area of the valve regulates the pressure drop across the valve, and therefore, provides the desired load to the system. In the incompressible approach, the flow difference across the piston of the load cylinder is assumed to be the same as that across the flow control valve. The fluid flowing through the valve orifice is forced by the motion of the piston. The following relations formed the dynamic

model of the load simulator (Zhang. Q., J. F. Reid, and D. Wu, 2000).

$$Q_p = c_d A_{pv} \sqrt{\frac{2}{\rho}(P_{p1} - P_{p2})} \quad (1)$$

$$Q_p = A_p \dot{y} \quad (2)$$

$$F_p = \frac{\rho A_p^3}{2c_d^2}\left(\frac{\dot{y}}{A_{pv}}\right)^2 sign(Q_p) \quad (3)$$

where $Q_p$ flow rate across the load control valve (m³/s), $C_d$

valve orifice coefficient, $A_{pv}$ orifice area of the load control valve

(m²), ρ fluid mass density (kg/m³), P pressure in both chambers of

the steering cylinder (Pa), $A_p$ cylinder area of the load cylinder (m²),

and $\dot{y}$ velocity of steering actuator
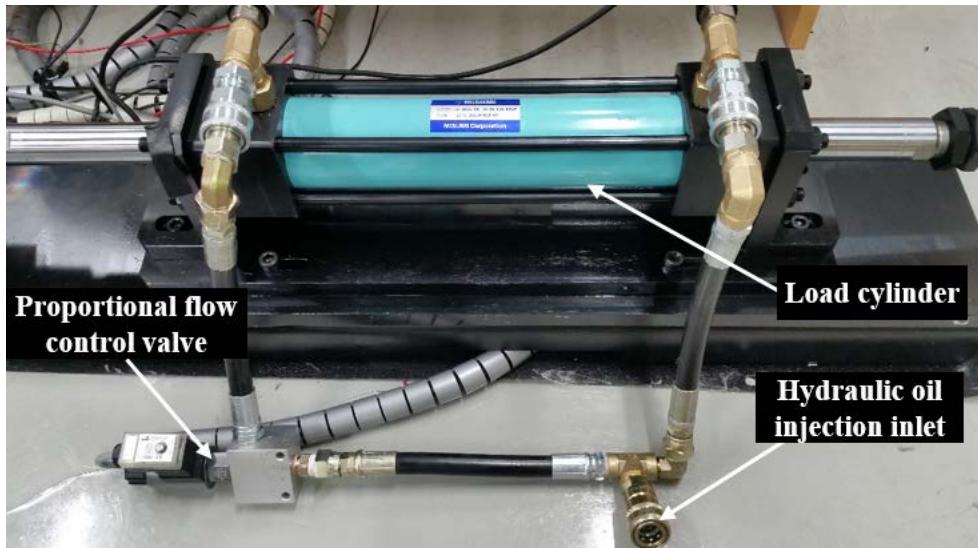
**Fig. 24 Configuration of the loader system.**
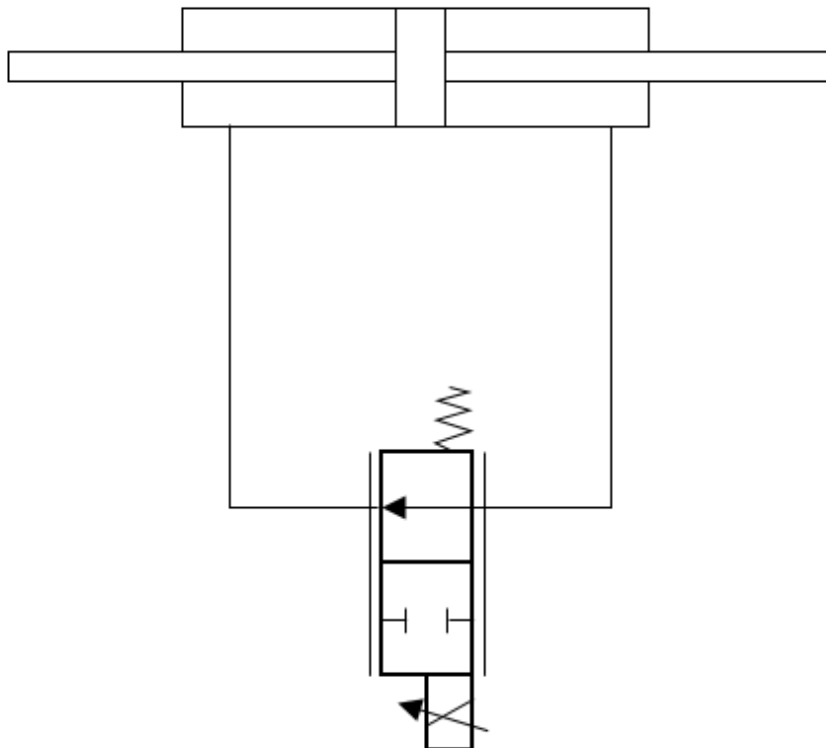


**Fig. 25 Hydraulic circuit of the loader system.**

## 2.3.  ISO 11783 Network

### 2.3.1.  ISO 11783 (ISOBUS)

ISO 11783, also known as ISOBUS, is a CAN higher layer protocol based on the SAE J1939 standard for forestry and agricultural vehicles. The primary goal of ISOBUS is to standardize the communication which takes place between tractors and implements while ensuring full compatibility of data transfer between the mobile systems and the office software used on the farm. Instead of different control boxes in the cab, ISOBUS allow the operator to use one display for an entire fleet of implements. Fig. 26 shows different control units for Non-ISOBUS implements.

ISO 11783 was a joint development by manufacturers in the agricultural and forestry industry to address the increasing needs for electronic control in the machinery and vehicles they produce. The conformance tests are performed by AEF accredited test laboratories. When a device passes the conformance tests it then receives an AEF ISOBUS Certification label which not only shows that the device conforms to ISO 11783 standard and AEF design guidelines but also the functionalities the device supports. Fig. 27 shows ISOBUS certification label.

**Fig. 26 Many 'island' solutions to operate implements or perform other tasks**



**Fig. 27 AEF ISOBUS certification label**

ISO 11783 supports two or more network segments. One segment is identified as the tractor network. This segment is intended to provide the control and data communications for the drive train and chassis of the tractor or primary power unit in a system. The second segment is identified as the implement network that provides the control and data communications between implements, and between implements and the tractor or main power unit in the system. Fig. 28 illustrates the topology of a typical network in agriculture and forestry that uses serial control and communications data.

As shown in Fig. 29, in this study, a network topology of four ECUs was designed based on ISO 11783 standard: a steering ECU, an EHPV, an EPS, and a virtual terminal (VT). Table 4 shows the communication databases between ECUs (ISO. 11783-7).

The steering ECU determines a direction and an amount of flow commands according to Target Angle message (0x600) and steered wheel angle data from the potentiometer, and Auxiliary Valve Command message (PGN: 65072) is sent to the CAN bus. The EHPV built in a PVED-CC that is a digital controlled actuator for PVG 32, which is compliant to the ISOBUS standard for flow control. The EHPV receives Auxiliary Valve Command message via CAN bus, and

controls solenoid spool valve. The EPS receives Target Angle

message (0x600) via CAN bus, and a current from the motor drive

circuit to the EPS motor is controlled by PID controller within the

target current amount, and the motor operates accordingly. The VT

provides a capability to display information and to retrieve data from

an operator. A detail description of the VT follows section 2.5.
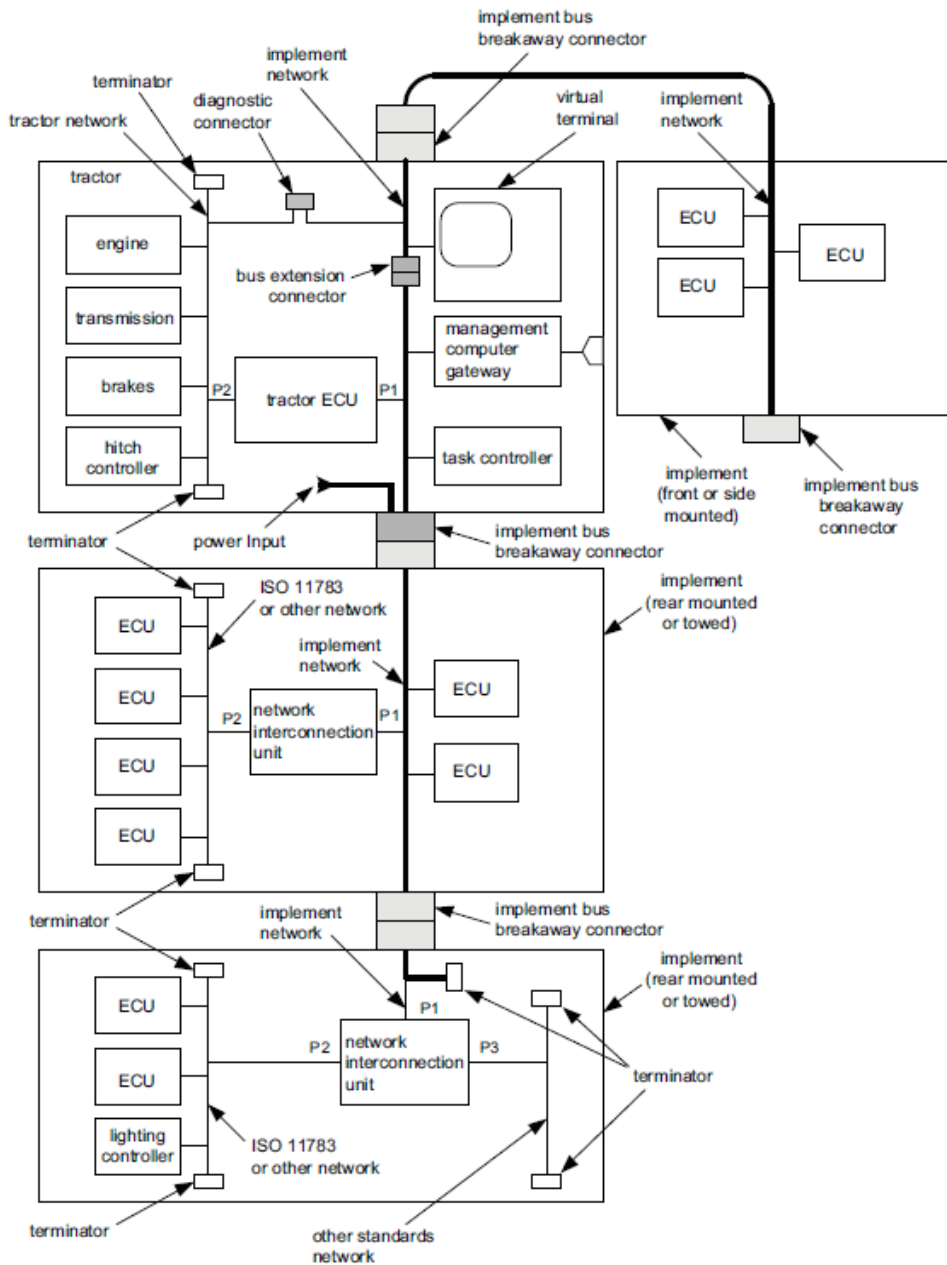
**Fig. 28 Typical ISO 11783 network**

41
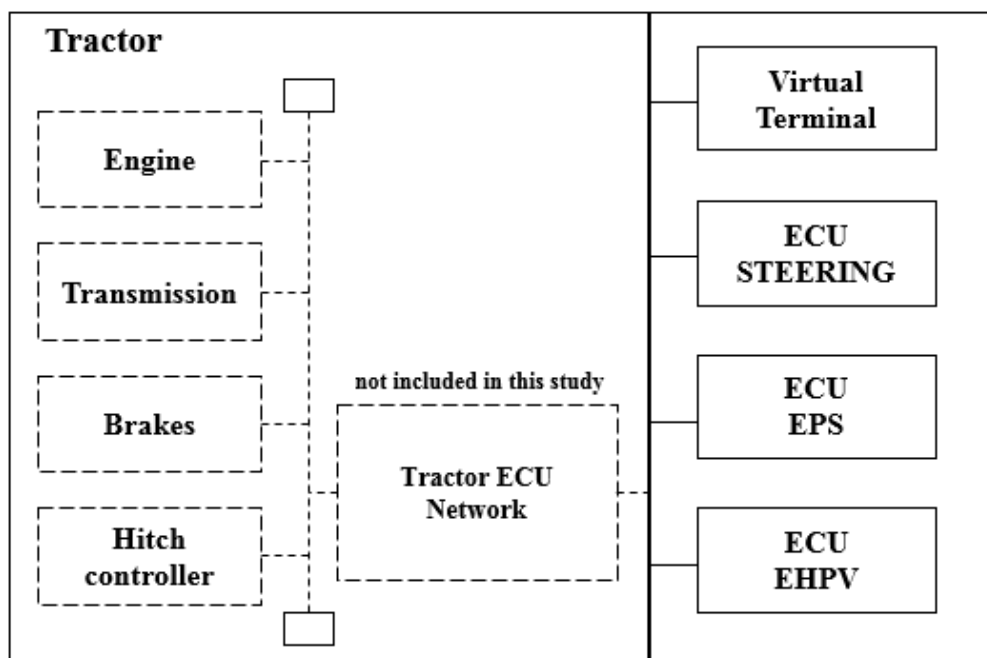
**Fig. 29 Topology of the steering system**

**Table 4 Communication database for CAN.**

| 1. GNSS Position Rapid Update (IEC 61162-3) | | | |
|---|---|---|---|
| PGN | 129025 | DLC | 8Byte |
| 0~3Byte | Latitude (Value Type: Signed, Unit: deg ) | | |
| 4~7Byte | Longitude (Value Type: Signed, Unit: deg ) | | |

| 2. Speed (IEC 61162-3) | | | |
|---|---|---|---|
| PGN | 128259 | DLC | 8Byte |
| 0Byte | Sid (Value Type: Unsigned) | | |
| 1~2Byte | Speed Water Reference (Value Type: Unsigned ) | | |
| 3~4Byte | Speed Ground Reference (Value Type: Unsigned, Unit: m/s ) | | |

| 3. Vessel Heading (IEC 611262-3) | | | |
|---|---|---|---|
| PGN | 127250 | DLC | 8Byte |
| 0Byte | Sid (Value Type: Unsigned) | | |
| 1~2Byte | Heading Sensor Reading (Value Type: Unsigned, Unit: rad ) | | |
| 3~4Byte | Deviation (Value Type: Signed, Unit: rad ) | | |
| 5~6Byte | Variation (Value Type: Signed, Unit: rad ) | | |
| 7Byte 56~57bit | Heading Sensor Ref (Value Type: Unsigned ) | | |

| 4. Attitude (IEC 61162-3) | | | |
|---|---|---|---|
| PGN | 127257 | DLC | 8Byte |
| 0Byte | Sid (Value Type: Unsigned ) | | |
| 1~2Byte | Yaw (Unit: rad ) | | |
| 3~4Byte | Pitch (Unit: rad ) | | |
| 5~6Byte | Roll (Unit: rad ) | | |

5. Target Angle (Not follow ISO 11783 standard)

| ID | 0x600(11bit) | DLC | 3Byte |
|---|---|---|---|

| 0Byte | Mode (01: Mode on, 00: Mode off ) |
|---|---|
| 1~2Byte | Target Angle (Value Type: Signed, Unit: deg ) |

6. Primary Steered Wheel Angle (Not follow ISO 11783 standard)

| ID | 0x105(11bit) | DLC | 2Byte |
|---|---|---|---|

| 0~1Byte | Position (Value Type: Unsigned, Unit: deg ) |
|---|---|

7. Guidance System Command (ISO 11783-7)

| PGN | 44288 | DLC | 8Byte |
|---|---|---|---|

| 0~1Byte | Curvature Command (Value Type: Unsigned ) |
|---|---|
| 2Byte bits 2~1 | Steering Command Status (00: not intended for steering, 01: intended for steering ) |
| 2Byte Bits 8~3 | Reserved |
| 4~7Byte | Reserved |

8. Auxiliary Valve Command (ISO 11783-7)

| PGN | 65072 | DLC | 8Byte |
|---|---|---|---|

| 0Byte | PFC (Unit: 0.4%/bit) |
|---|---|
| 1Byte | Reserved |
| 2Byte | Bits 8~7: Fail Safe Mode<br>Bits 6~5: Reserved<br>Bits 4~1: Valve State |
| 3~7Byte | Reserved |

## 2.4.    Steering Control Algorithm

Hydraulic control system are used in most industries where heavy objects are manipulated or large forces are exerted on their surroundings. However, the rather complex structure of such systems makes it difficult to develop suitable, preferably low-order models of the dynamic of the plant (Jelali. M., and H. Schewarz. 1995). Hydraulic servo systems consist of components such as servo valves, actuators and pumps whose dynamic characteristics are complex, nonlinear and time-varying. Conventional controller design based upon linearized time invariant models may not guarantee satisfactory performance due to variation of the operating point (Ziaei. K, 1998).

Nonlinearities are of particular importance in hydraulic control. In most nonlinear systems the problem is one of determining the effect on performance of certain nonlinear elements. No general nonlinear theory exists, but there are several techniques which are applicable to certain classes of problems.

This section describes the development of a steering controller for vehicles equipped with an EH steering system. An EHPV was used as an orifice valve to supply different flow rates to the steering cylinder by changing the displacement of the spool (driven by a solenoid),

according to the specified of oil flow, which ranges from 0 to 250, through the CAN bus. As shown in Equation (4), the flow across each orifice in a hydraulic valve was generally given using an orifice equation. The dynamic viscosity of a liquid varies considerably with the temperature, and thus a hydraulic fluid has a significant impact on the operation of a hydraulic system, specifically at low temperatures. The effect of temperature on the dynamic viscosity is also described through Equation (5). The discharge coefficient depends on the geometry of the conduit and on the Reynolds number which can be approximated using Equation (6).

$$Q = C_d A_n \sqrt{\frac{2}{\rho} \Delta P} \qquad (4)$$

$$\eta = \eta_0 e^{-\lambda(\theta - \theta_0)} \qquad (5)$$

$$C_d = \frac{1}{\sqrt{\frac{k_1}{\frac{\rho v d_h}{\eta}} + k_2}} \qquad (6)$$

where Q is the flow rate across the orifice, $C_d$ is the discharge coefficient which is dependent on the Reynolds number, $A_n$ is the flow section area, $\rho$ is the oil density, $\Delta P$ is the pressure drop across an orifice, $\lambda$ is the viscosity-temperature coefficient, $\eta$ and $\eta_0$ are the dynamic viscosity at reference temperature $\theta$ (℃) and $\theta_0$ (℃), $d_h$ is the hydraulic diameter, v is the average flow velocity, and $k_1$ and $k_2$ are

constant values.

In this study, a proportional-feedforward architecture was applied for the steering controller, as shown in Fig. 30. Compared with feedback control, feedforward control has an advantage in that corrective actions may be applied before a disturbance has influenced the variables. Thus, feedforward control allows rapid reference tracking without affecting the system stability of the system. A nonlinear compensator consists of dead time, dead band, and static friction compensators, and the setpoint of the EHPV for the steering control algorithm is shown in Equation (7). Detailed descriptions of the nonlinear compensator are given belows.
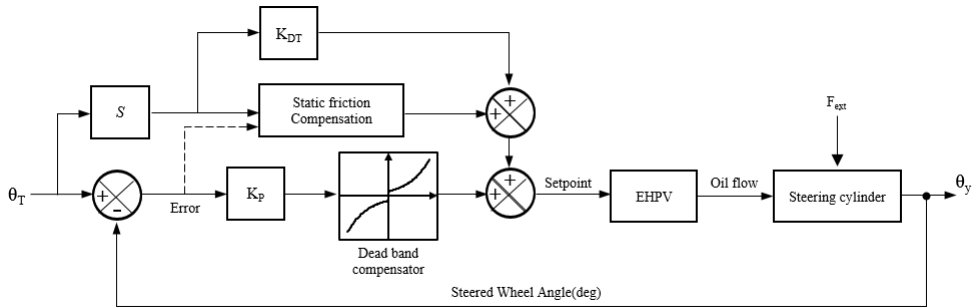


**Fig. 30 Block diagram of the steering controller.**

$$\text{Setpoint} = Setpoint_{dead-time} + Setpoint_{dead\ band} + Setpoint_{static\ friction} \qquad (7)$$

## 2.4.1. Dead Time

Many processes in industry, as well as in other areas, exhibit dead times in their dynamic behavior. Considering dead times are integral part of process dynamics systems. Dead times are mainly caused by information, energy or mass transportation phenomena, but they can also be caused by processing time or by the accumulation of time lags in a number of simple dynamic systems connected in series (Normey-Rico. J. E., and E. F. Camacho, 2007).

For processes exhibiting dead time, every action executed in the manipulated variable of the process will only affect the controlled variable after the process dead time. For this reason, the analysis and design of a controller for a dead-time system are more difficult to achieve. Fig. 31 shows typical behavior of a dead-time element.
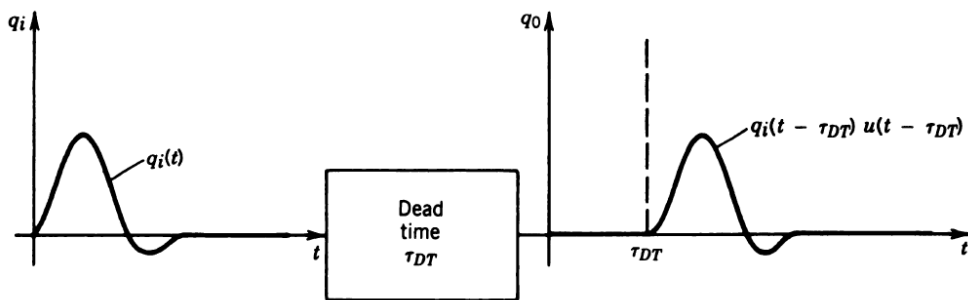


**Fig. 31 Dead time element.**

Following a study on an approximation of the dead time (Doebelin, E. O, 1985), a simple dead-time approximation for the control system was used, which is shown in Fig. 32. In principle, the Laplace transfer function of the dead-time elements can be defined as follows:

$$q_o(t) = q_i(t - \tau_{DT}) \qquad (8)$$

$$\frac{Q_o}{Q_i}(s) = e^{-\tau_{DT}s} \qquad (9)$$

where $q_i$ is the input (target angle, $\theta_r$) variable of physical system, $q_o$ is the output (steered wheel angle, $\theta_y$) variable of physical system, $Q_i$ and $Q_o$ are the Laplace transform of the time functions $q_i$ and $q_o$, and $\tau_{DT}$ is the constant dead-time value.

The simplest dead-time approximation can be obtained by applying the Taylor series expansion of Equation (9), which is given in Equation (10). When converting the s-domain into the time domain, errors caused by the dead-time effect can be obtained as described in Equation (11). That is, an error caused by the dead-time effect can be calculated using the product of the dead-time and the derivative of $q_i$. As a result, it is expected that an inherent error caused by a dead-time will be manly affected by the derivative of the input variable. The

dead-time compensation values of the EHPV for the steering control

algorithm are shown in Equation (12).

$$Q_o(s) \cong (1 - \tau_{DT}s)Q_i(s) \qquad (10)$$

$$q_i(t){-}q_o(t) \cong \tau_{DT}\frac{dq_i(t)}{dt} \qquad (11)$$

$$Setpoint_{dead-time} = \tau_{DT}\frac{dq_i(t)}{dt} \qquad (12)$$
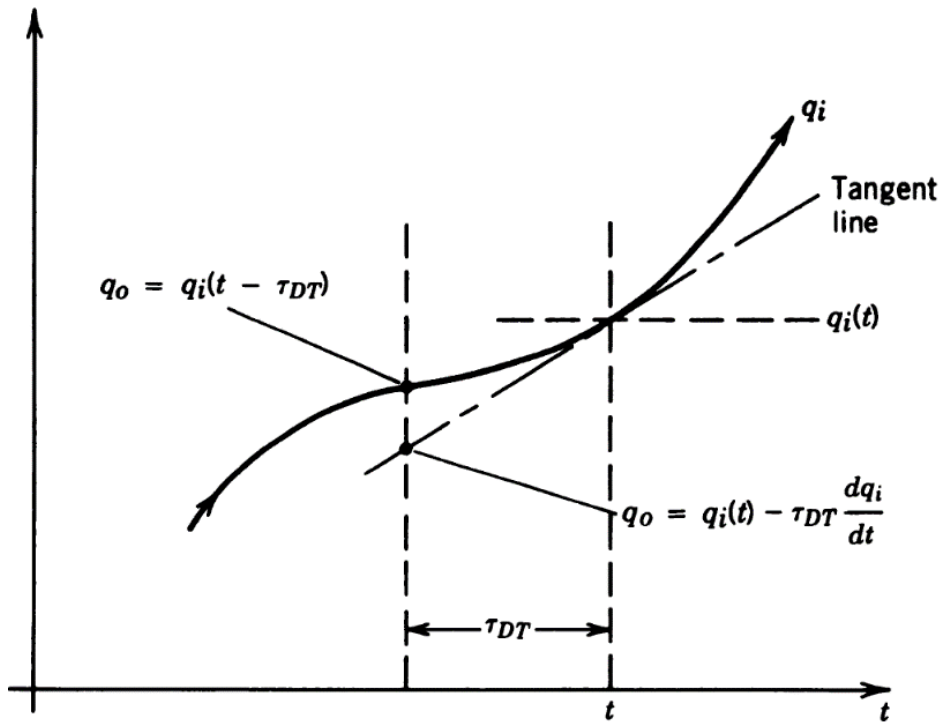


**Fig. 32 Dead-time approximation.**

### 2.4.2. Dead Band

Closed center or overlapped valves have a land width greater than the port width when the spool is neutral. The fully closed center cross-over may cause backlash, and so undesirable pressure peaks occur in the system which vary with amount of fluid flow and switching time(Jelali, M., and A. Kroll, 2002, Fig. 33).
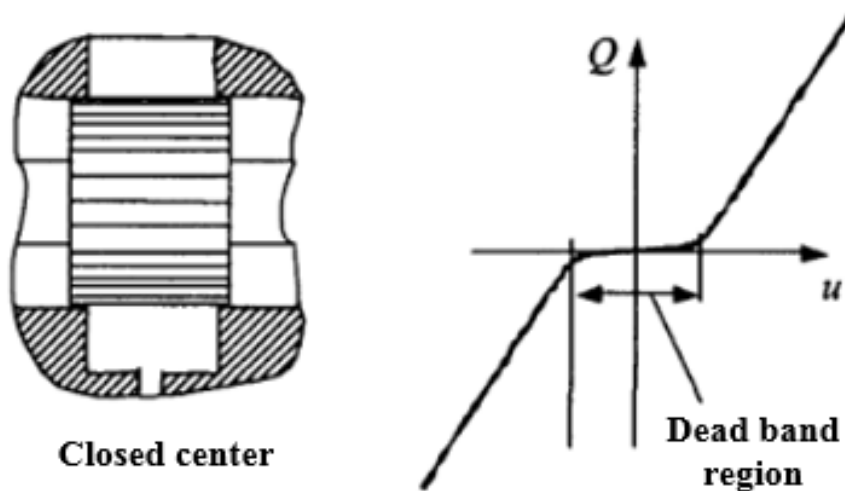


**Fig. 33 Definition of closed center valve.**

A dead band nonlinearity can result from coulomb friction and from overlap of valve ports in hydraulic systems. The presence of a dead band is a disadvantage for valve control: when a dead band is present, small voltages do not actuate the rod, but when the voltage exceeds a certain threshold and the rod initiates its motion, the position error has already grown excessively and the controller

overreacts by displacing the rod at high speed to compensate for the error (Mas, F. R., and Z. Qin, and A. C. H, 2010).

The nonlinear gain function is the static relationship between the input and the output of the system. It can be obtained experimentally from a series of response test on the open loop system (Qiu, H. C., Q. Zhang, J. Reid, and D. Wu. 1999).

This method can be mathematically expressed as Equation 13.

$$G_p(s) = f_n(u)G_l(s) \quad (13)$$

where $G_p(s)$ is the open-loop transfer function, $G_l(s)$ a linear transfer function, and $f_p(u)$ the nonlinear gain function of the E/H steering system.

The nonlinear gain function is a valve transform that consists of information regarding the nonlinearity of an E/H valve. Fig. 34 shows the results of the characteristic curves of a steering valve under various oil flows, i.e., 9.5, 14.5, and 19.3 LPM. Using the HIL simulator, a valve transform was configured experimentally based on the relationship between the setpoint values of the EHPV and the corresponding steering rates. When the setpoint values are less than 35, the steering cylinder appears to fall into a non-response region. The reasons for the occurrence of a non-response region are mainly due to the influence of the dead band. Comparing the level of performance under three different oil flow conditions, similar

performance curves were obtained at flow rates of 14.5 and 19.3

LPM; however, a large difference was shown at 9.5 LPM. Because the

flow conditions of the tractor used in this study are within an

approximate range of about 14.6 to 21.1 LPM, the flow conditions

used in the simulator-based experiments were kept constant at

19.3LPM.

The linear model is used as the linear transfer function of the E/H

steering system. This model can be mathematically derived from

Equation 14 by introducing an inverse nonlinear gain function of the

system.

$$G_l(s) = f_n^{-1}(u)G_p(s) \qquad (14)$$

Fig. 35 shows the inverse transform of the steering valve. To

compensate the dead band of the steering valve, an inverse valve

transform model was identified using curve-fitting method.

$$y = 32.569e^{0.0408x}, R^2 = 0.9903 \qquad (15)$$

The inverse valve transform provides a non-linear control

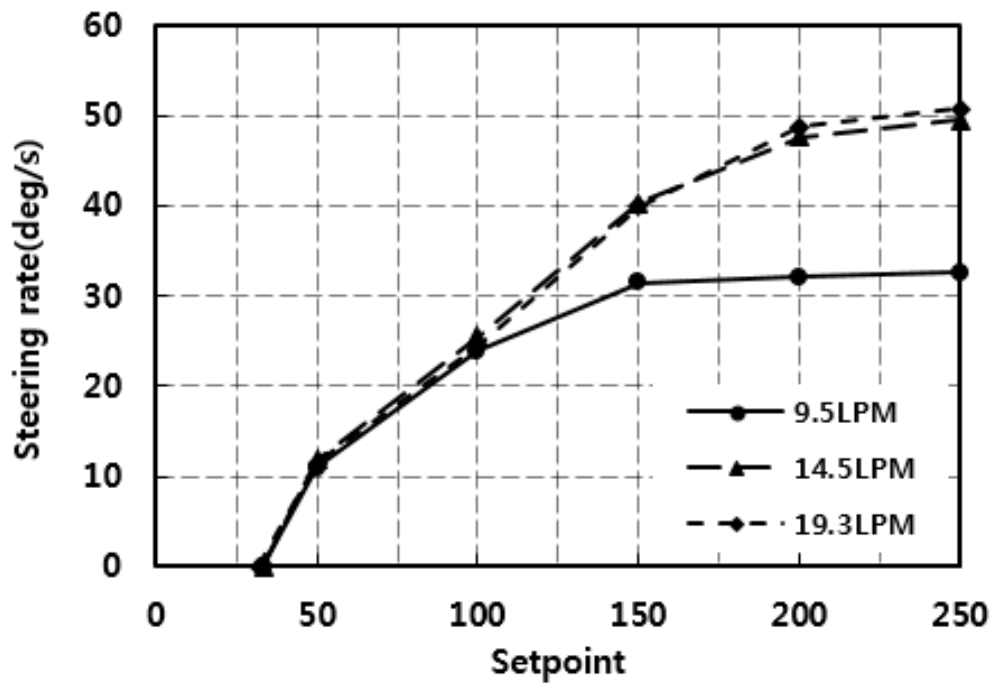command to quickly actuate the valve spool out of its dead zone.

**Fig. 34 Characteristic curves of steering valve at various oil-flow rates obtained experimentally from the HIL simulator.**
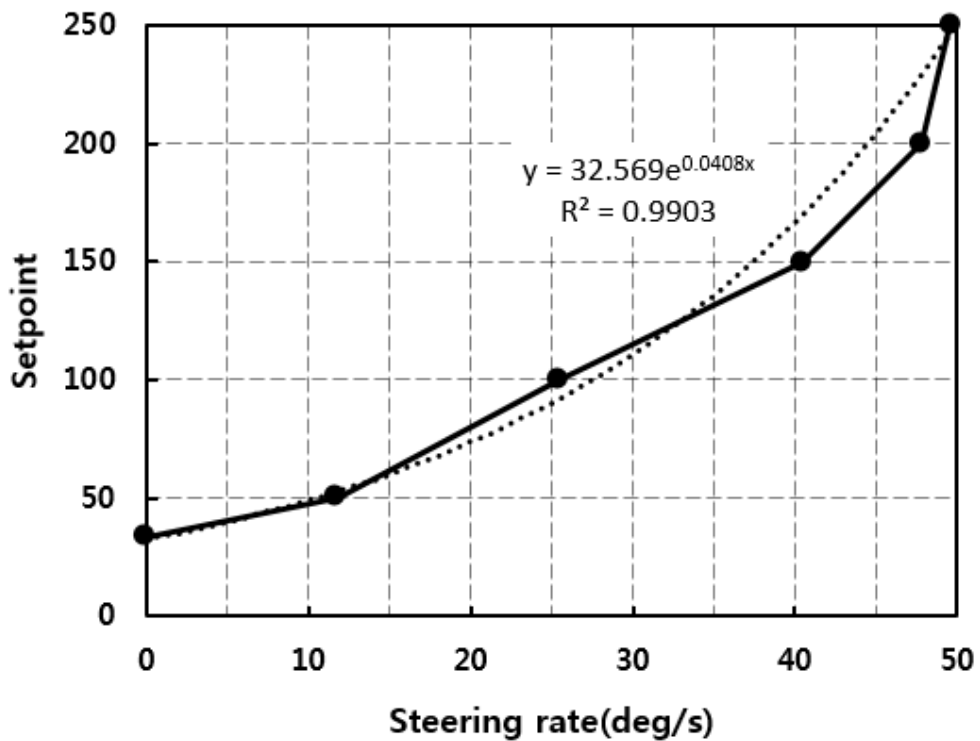


**Fig. 35 Inverse transform of the steering valve, and curve fitting model.**

As shown in Equation (16), in fluid dynamics, the volumetric flow rate and the piston speed have a linear relationship.

$$V = \frac{Q}{A_n} \qquad (16)$$

where $V\ [cm^3/s]$ is the piston speed, $Q[cm^3/s]$ is the pump flow rate, and $A_n\ [cm^2]$ is the piston area.

According to the spool characteristic curve, the setpoint and flow rate are linearly related. Therefore, the setpoint and piston speed also have a linear relationship. Based on the maximum steering rate of $\pm 50$ deg/s, the output of the P controller was configured to be the input to the inverse transform within the range of -250 to 250. Fig. 36 shows the dead-band compensation model. The dead-band compensation values of the EHPV for the steering control algorithm are shown in Equation (17).

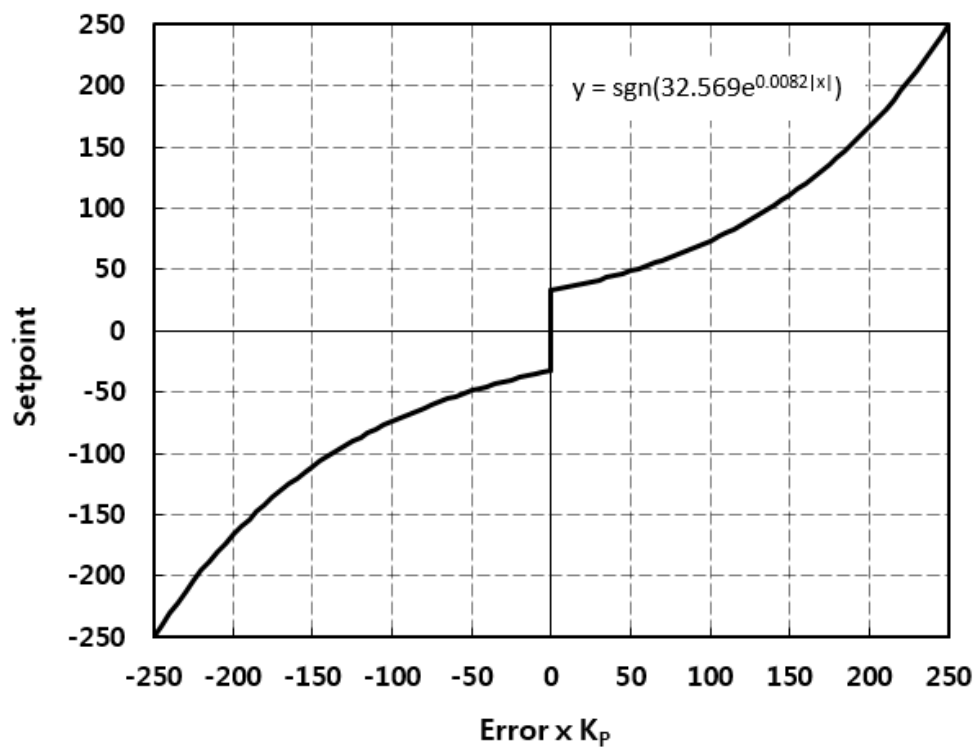$$Setpoint_{dead\ band} = K_p sgn(32.569e^{0.0082|x|})(\theta_{error}) \quad (17)$$

**Fig. 36 Dead-band compensation model.**

### 2.4.3. Static Friction

There are many sources of friction in such a steering system, including cylinder piston, and the load and side load caused by the road wheels. The friction is highly nonlinear and may adversely affect the performance of the steering control system resulting in steady state errors, limit cycles, and stick-slip motion. Consequently, the road wheels may not follow the steering wheel command as desired. One of the main non-linearities of the cylinder is non-linear friction. Depending on the application, Coulomb friction and stiction phenomena may have a particularly significant effect on the controller's performance (Jelali, M., and A. Kroll, 2002). Robotic manipulators must contend with friction which poses a serious challenge to precise manipulator control. Specifically, failing to compensate for friction can lead to tracking errors when velocity reversals are demanded and oscillations when very small motions are required (Leonard. N. E, and P. S. Krishnaprasad, 1992). Coulomb friction is present in hydraulic cylinder seals, although it is only one of the components constituting seal friction characteristics. The basic lubrication mechanism of seals is shown in Fig. 37. It can be seen that the fiction force versus velocity curve is non-linear, particularly at low
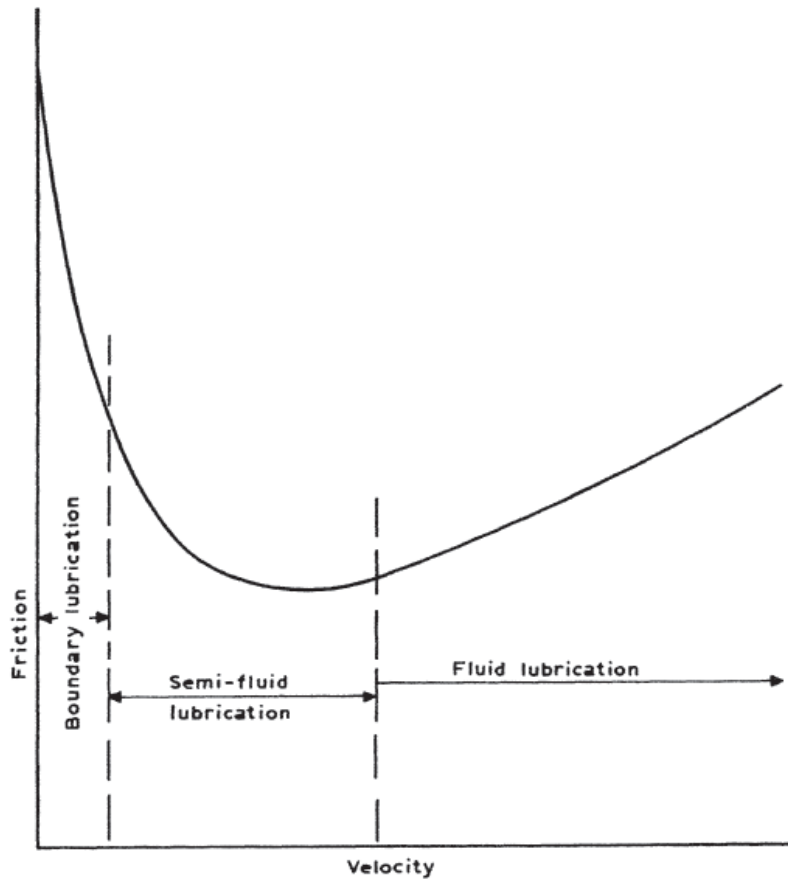
cylinder velocities.



**Figure 37 Lubrication mechanism of sliding surfaces**

To overcome the static friction of a steering cylinder, an impulse-based compensator was proposed in the feedforward loop when the controller received a new steering command for a directional change (Qiu. H. and Q. Zhang, 2003).

In this study, the impulse-based compensator used by Qiu et al. was applied to compensate the static friction of the cylinder. Static friction is the friction that occurs between two or more solid objects

that are not moving relative to each other. In a steering system, static friction appears mainly at the beginning of the change in the direction of the cylinder. Static friction is a problematic in that the controller overreacts by displacing the rod at high speed to compensate for any errors that may occur.

In this study, a simple method is proposed for compensating the static friction that occurs when the direction of the cylinder is changed. Fig. 38 shows the algorithm used for compensating the static friction during changes in direction. A differentiator of the target angle was used to obtain the direction information of the cylinder. To determine the exact time at which an error occurs from static friction, a threshold value of the steering angle error was set. Impulse mode was activated when the threshold value was exceeded, and during the preset duration (d), a high-magnitude impulse (I) was instantaneously generated to convert the static friction into kinetic friction, as shown in Equation (18). A period of 0.06 s (d) and a magnitude of 80 were found to be sufficient parameters to overcome the static friction in this study, and where the threshold value ($e_{thres.}$) was set to $0.2°$. The static friction compensation values to the EHPV for the steering control algorithm are shown in Equation 19.

$$Impulse(t) = \begin{cases} I, & (t_0 \leq t \leq t_0 + d) & if\ \theta'_T > 0 \\ -I, & (t_0 \leq t \leq t_0 + d) & if\ \theta'_T < 0 \\ 0, & (t > t_0 + d) & otherwise \end{cases} \quad (18)$$

$$Setpoint_{static\ friction} = Impulse(t) \quad (19)$$

where I is the impulse amplitude, d is the impulse duration, and

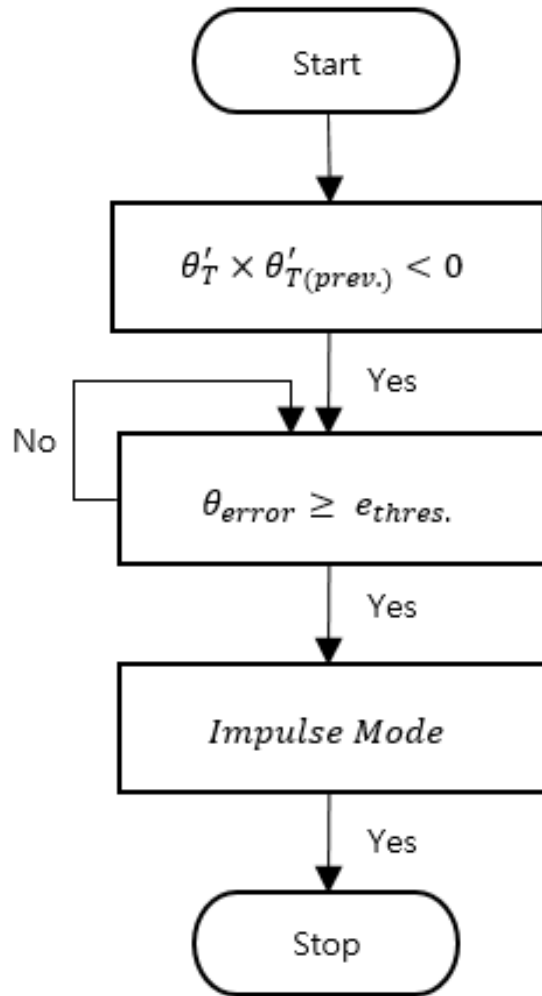$t_0$ is the time when the threshold value is exceeded.



**Fig. 38 Flow chart of static friction compensator.**

## 2.5. Virtual Terminal

A virtual terminal (VT) is a device for operator interaction with the features of the tractor and agricultural implement. The VT is a control function within an electronic control unit (ECU), consisting of a graphical display and input functions, connected to an ISO 11783 network that provides the capability for a control function, composing an implement or a group of implements to interact with an operator. As shown in Fig. 39, the VT provides the capability to display information and to retrieve data from an operator (ISO 11783-6).



**Fig. 39 A VT provides ISO 11783 systems with a graphical display, soft keys, and means to retrieve user inputs**

In this study, the VT was constructed to set the auto steering mode as well as to receive the status information of the vehicle in real time. The virtual terminal used a commercial OPUS A3 Eco model (WACHENDORFF Elektronik, Germany). The VT features 32-bit, 532 MHz processor, with memory 512 MB and two CANBUS ports.

Projektor Tool software is tailored to fit into the ISOBUS development tool chain. Projektor Tool software development suite with graphics development tools and JavaScript capability can be used to reduce programming time. Fig. 40-41 shows screenshot of the Projektor Tool software.
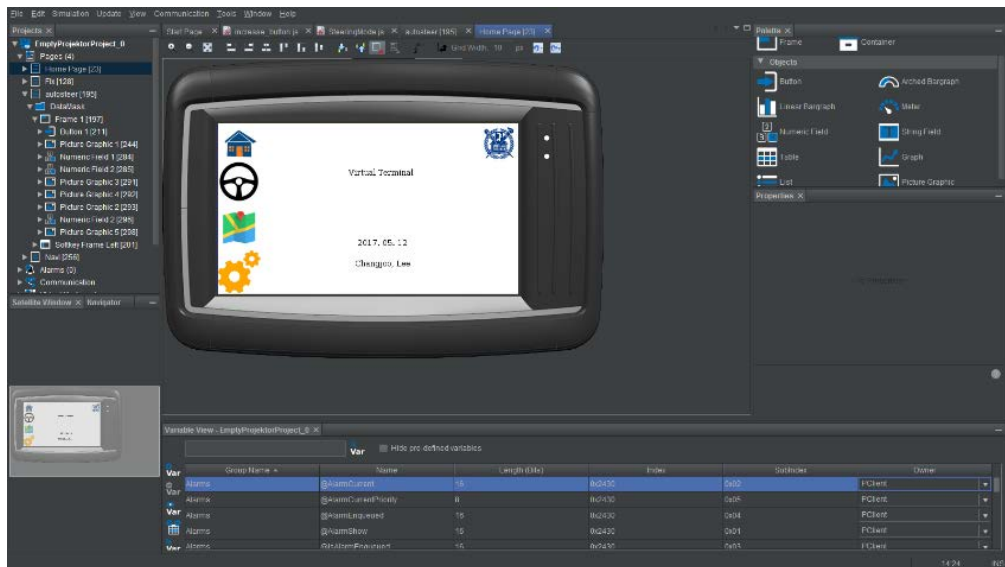
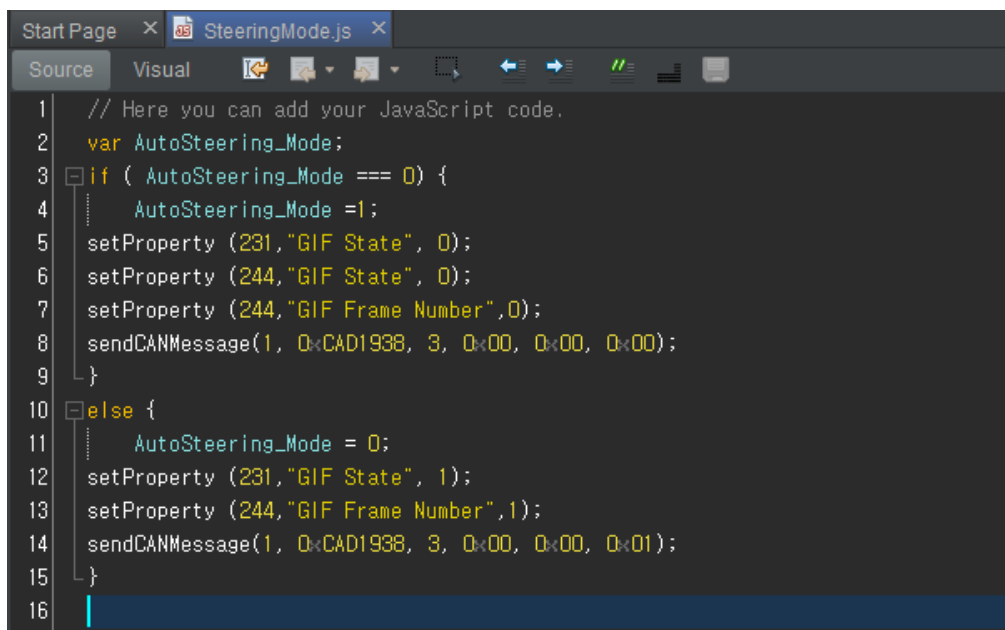**Fig. 40 Screenshot of the Projektor Tool software.**



**Fig. 41 Screenshot of programming language.**

The user interface of the VT consists of main, auto steering status, and positioning status. The main tab is for selecting the other tabs. The auto-steering status tab is shown in Fig. 42. From the auto steering status tab, the user can start or stop the auto steering mode. After the auto steering mode is turned on, the VT sends the message of the guidance system command (PGN 44288). In addition, the VT may real-time receive the vehicle speed, steered wheel angle, and target angle information from CAN bus: Target Angle (0x600), Primary Steered Wheel Angle (0x105), and Speed (PGN 128259).
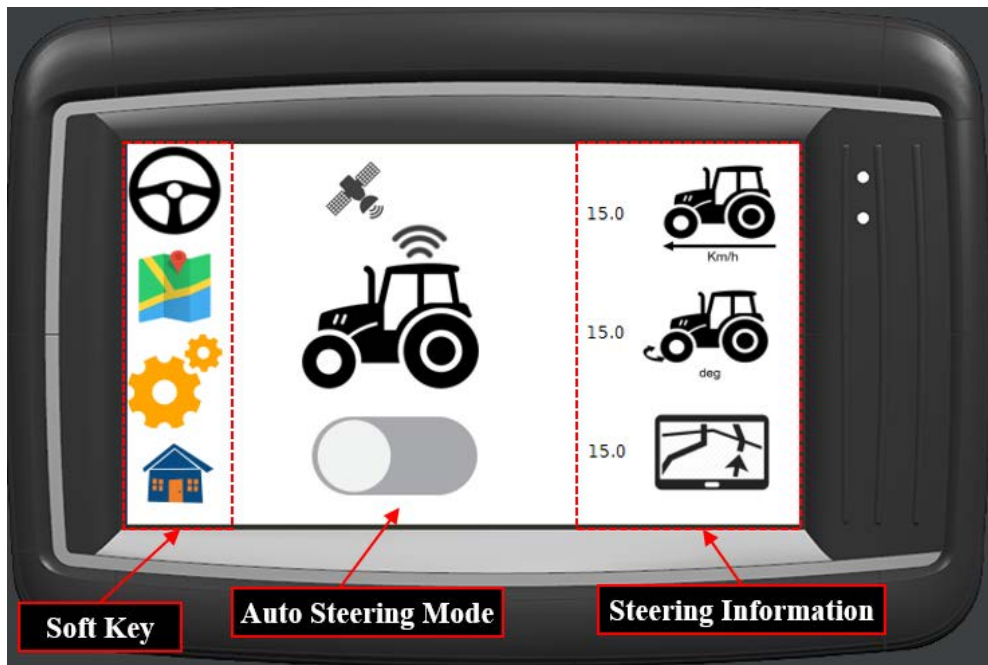


**Fig. 42 The auto steering status tab of the VT contains two functions; activation of the auto steering mode, reading steering information.**

The positioning status tab shown in Fig. 43 contains the vehicle heading, vehicle speed, latitude, and longitude information. The VT is configured to receive CAN messages according to the IEC 61162-3 standard: GNSS Position Rapid Update message (PGN 129025), Speed (PGN 128259), and Vessel Heading (PGN 127250).
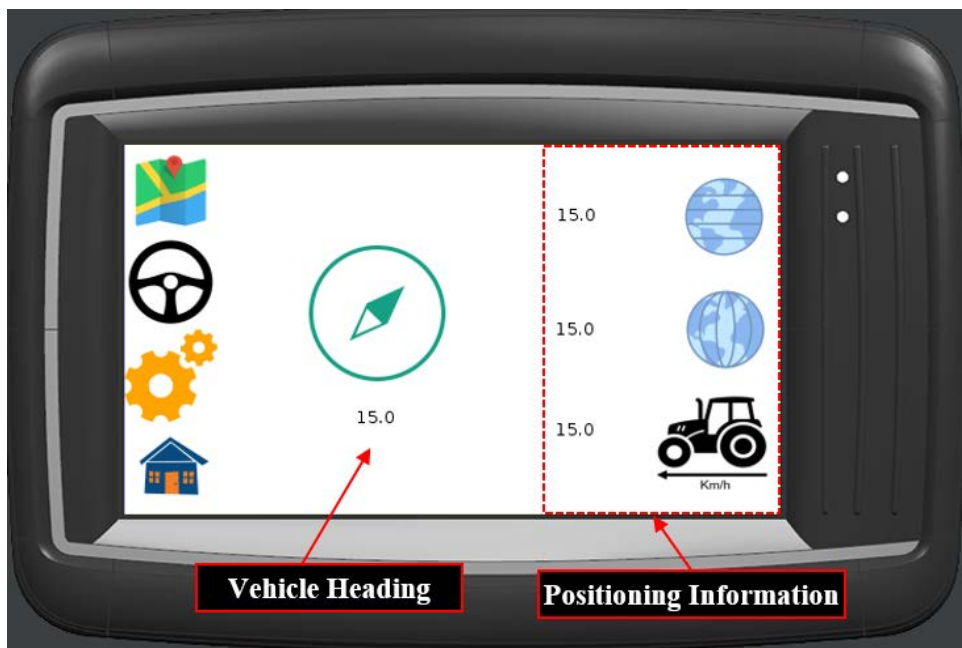


**Fig. 43 The positioning status tab of the VT contains vehicle heading and positioning information**

## 2.6. Vehicle Traveling Test

### 2.6.1. Hardware Configuration

As shown in Fig. 44, the steering circuit used in the HIL simulator was applied to the tractor in the same manner. The tractor used for this experiment used an open center hydraulic circuit based on a hydrostatic valve, and an EHPV and a directional control valve were additionally mounted through a hydraulic hose (Fig. 45). A gear pump was used to produce flow, and oil was allowed to pass through the EHPV or directional valve to the hydrostatic valve (P-line).

As shown in Fig. 46, a control box was configured to supply power to the controllers, sensors, valves, and other elements. In addition, a relay module was installed to control the on / off of state the directional control valve, and was controlled using a digital signal (12V, 24mA) output from VN8910A.

The configured EPS-based steering system uses 500kBaud, and the EHPV uses 250kBuad, and thus two CAN channels were applied. CAN channel#1 connected the EPS-based steering system, the path tracking system, whereas the VT, and CAN channel#2 connected the EHPV. Fig. 47 shows a photograph of the VT mounting location.

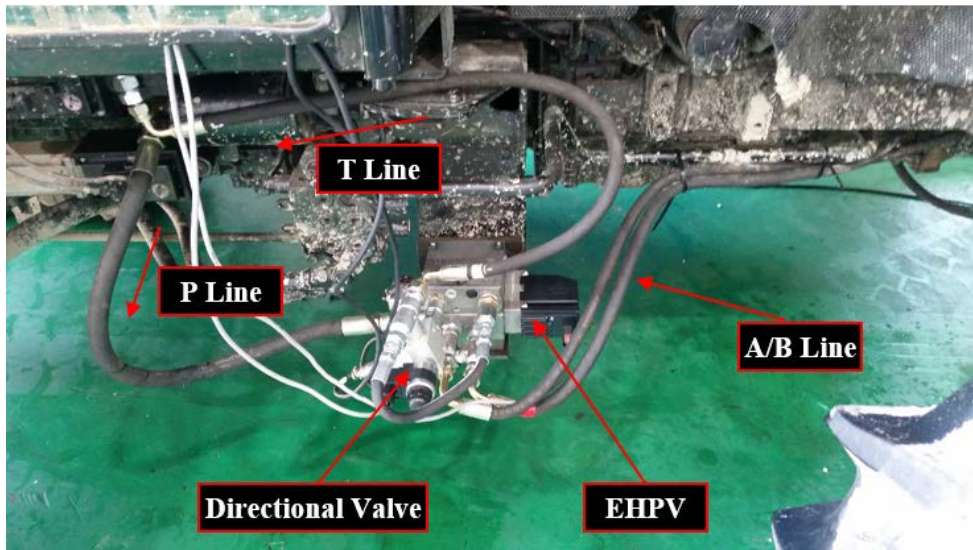**Fig. 44 Schematic view of steering system of the circuit**
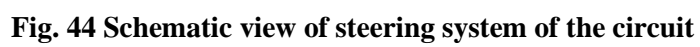
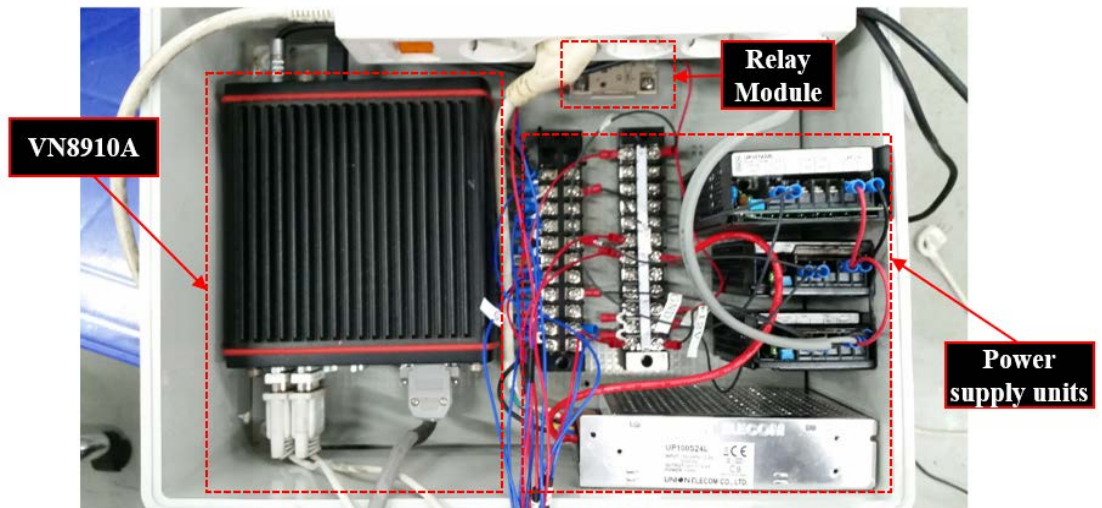**Fig. 45 Photograph of the EHPV and directional valve mounting position.**



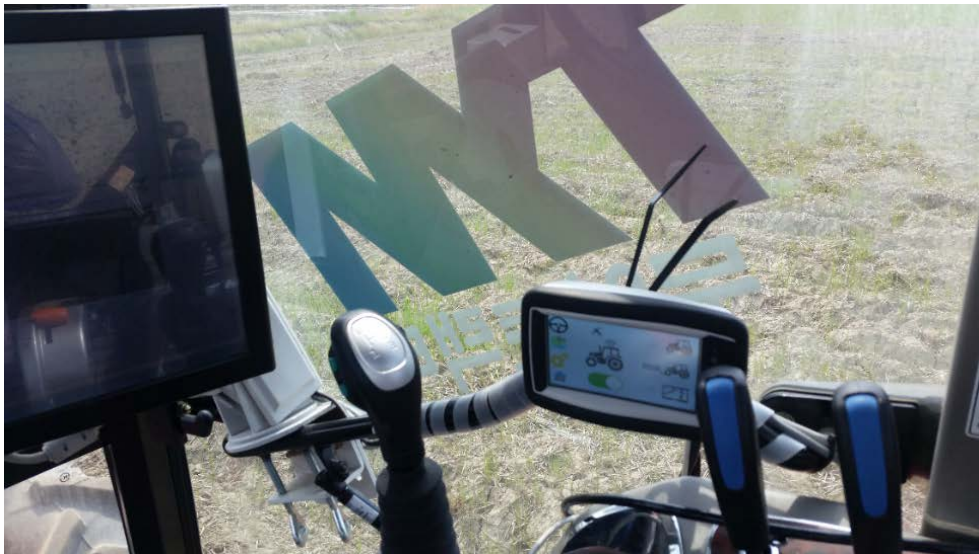**Fig. 46 Control box installation and configuration.**

**Fig. 47 Photograph of the VT mounting location.**

In this study, an auto-guidance system developed by Han (2017) was applied. A Real Time Kinetic (RTK)-GPS used in the auto-guidance system was connected to an interface console through RS232 communication, received the position information, and generated a path tracking algorithm (Fig. 48). The Steered wheel angle and speed information were sent to the interface module through a CAN, and were used to calculate the path tracking (Han, 2017). To obtain the GPS coordinates, a 42G1215A-Xt-1-2-CERT antenna and an OEM-617-D receiver were used. The antenna received correction signals through L1 and L2. The GPS receiver was able to achieve a precision level of up to 1 to 2 cm. Fig. 49 shows the RTK reference station installed on a farm.
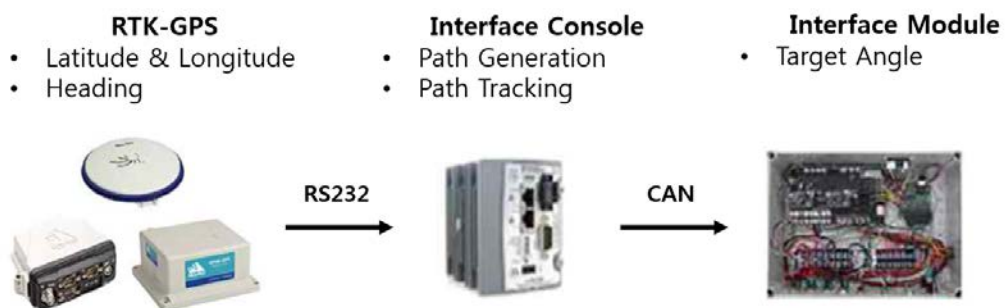


**Fig. 48 Configuration of the path-tracking system (Han, 2013).**

**Fig. 49 Photograph of RTK base station.**

**Table 5 Hardware specifications of the navigation system**

| Name | Specifications |
|---|---|
| **RTK Base** | − FlexPak-G2-V2 <br> − Signal Tracking : L1, L2 <br> − Horizontal position accuracy : <br> Single point L1: 1.5m <br> Single point L1, L2: 1.2m <br> DGPS: 0.4m <br> − RT-2: 1cm |
| **Rover** | − SPAN-CPT <br> − GPS Measurement : 5Hz <br> − GPS Position : 5Hz <br> − IMU Measurement : 100Hz <br> − IMU Performance : <br> Gyro Technology : FOG <br> Gyro Bias: 20deg/hr <br> Accelerometer Range: ±10g <br> Accelerometer Bias: 50mg |
| **Antenna** | − 701-GGL <br> − LNA Gain: 29dB <br> − Elementary Gain@Zenith <br> − L1: >5.0 dBi |

## 2.6.2.    Trajectory Tracking Control

The design of high performance control systems that assist in the navigation of the tractor requires understanding of steering dynamics. To simplify the analysis of the steering system, the four-wheel geometrical model is normally condensed into the bicycle model. Front and rear axles are both replaced by single virtual wheels, located at mid-distance between the actual wheels, shown in Fig. 50. Since the control objective is path following, the vehicle configuration is described with respect to the reference path C, rather than with respect to an absolute reference frame.
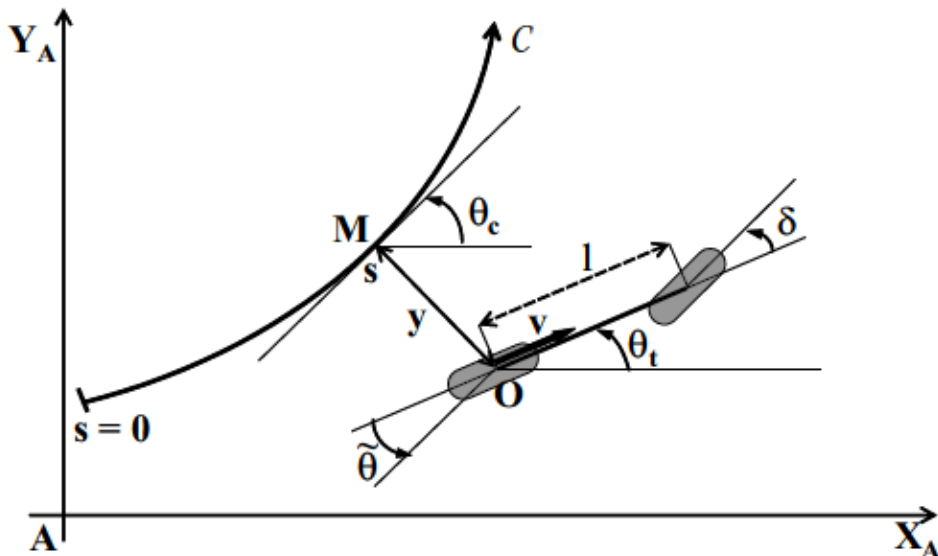


**Fig. 50 bicycle model description**

where C is the path to be followed, O is the center of the vehicle virtual rear wheel, M is the point on C which is the closest to O, s is the curvilinear abscissa of point M along C, c(s) denotes the curvature of path C at that point, $\theta_c$(s) stands for the orientation of the tangent to C at that point, $\tilde{\theta}$ is angular deviation of the vehicle, $\theta_t$ is the orientation of the tractor centerline, y is the lateral deviation of the tractor with respect to C, v is the tractor linear velocity at point O, L is the vehicle wheelbase, and $\delta$ is the orientation of the front wheel with respect to tractor centerline.

In this study, vehicle driving model based on Ackermann steering is designed without sliding conditions (Leonard. N. E, and P. S. Krishnaprasad, 1992, Han, X. Z., 2017).

$$\begin{cases} \dot{s} = \frac{vcos(\tilde{\theta})}{1-c(s)y} \\ \dot{y} = vsin(\tilde{\theta}) \\ \dot{\tilde{\theta}} = v\left[\frac{tan(\delta)}{L} - \frac{c(s)\cos(\tilde{\theta})}{1-c(s)y}\right] \end{cases} \qquad (20)$$

Using this model, a control law without sliding incorporated had been designed in based on chained system theory.

$$\delta(y,\tilde{\theta}) = \arctan(L\left[\frac{cos^3\tilde{\theta}}{(1-yc(s))^2}(-K_d(1-yc(s))tan\tilde{\theta} - K_p y + c(s)(1-yc(s))tan^2\tilde{\theta} + \frac{c(s)cos\tilde{\theta}}{1-yc(s)}\right]) \qquad (21)$$

### 2.6.3.    Zero-Load Test

To calibrate the parameters and measure the performance of the EHPV-based steering system, steering response experiments were carried out under no-load conditions, with a flow rate of about 10.5 LPM. Once the steady-state error was eliminated, a low-pass filter, with a cut-off frequency of 0.83 Hz, was implemented to try and improve the response of the steered wheel angle. As shown in Fig. 51, the front-wheel axle of the tractor was raised from the ground. The steering ECU provided step input commands through the EHPV, and the steered wheel angle.



**Fig. 51 Zero-load test conducted to calibrate and measure the performance of the EHPV-based steering system.**

### 2.6.4.     Sinusoidal Tracking Test

To analyze the steering performance of the tractor under actual soil conditions, sinusoidal tracking tests were conducted following a target angle with a sine wave of 0.25Hz. The travelling speeds were 2 and 5.5 km/h, and the EPS and EHPV steering systems were compared (Fig. 52). At 2km/h, the gear was set to low, and the flow rate was about 21.1 LPM. At a traveling speed of 5.5 km/h, the gears was set to high, and the flow rate was about 12 LPM. The experiments were repeated three times at the same location.



**Fig. 52 Photograph of sinusoidal tracking test.**

## 2.6.5.　　　Path Tracking and Test Methods

To compare the performance capabilities of both the EPS and the EHPV steering systems, actual path tracking tests were conducted. Traveling speeds of 2km/h, suitable for tillage and cutting, and 5.5 km/h, used for spraying and laying seeds, were applied.

As shown in Fig. 53, during the test, two experimental trajectories were constructed, i.e., Test 1 and Test 2, and the experiments were repeated three times at the same location.

For Test 1, the test trajectory consisted of three straight lines and two turns. The tractor's traveling speed was kept constant at 2km/h. The test trajectory for Test 2 consisted of a straight running route and the tractor maintained a speed of 5.5 km/h. Fig. 54 shows a photograph of the path-tracking test.
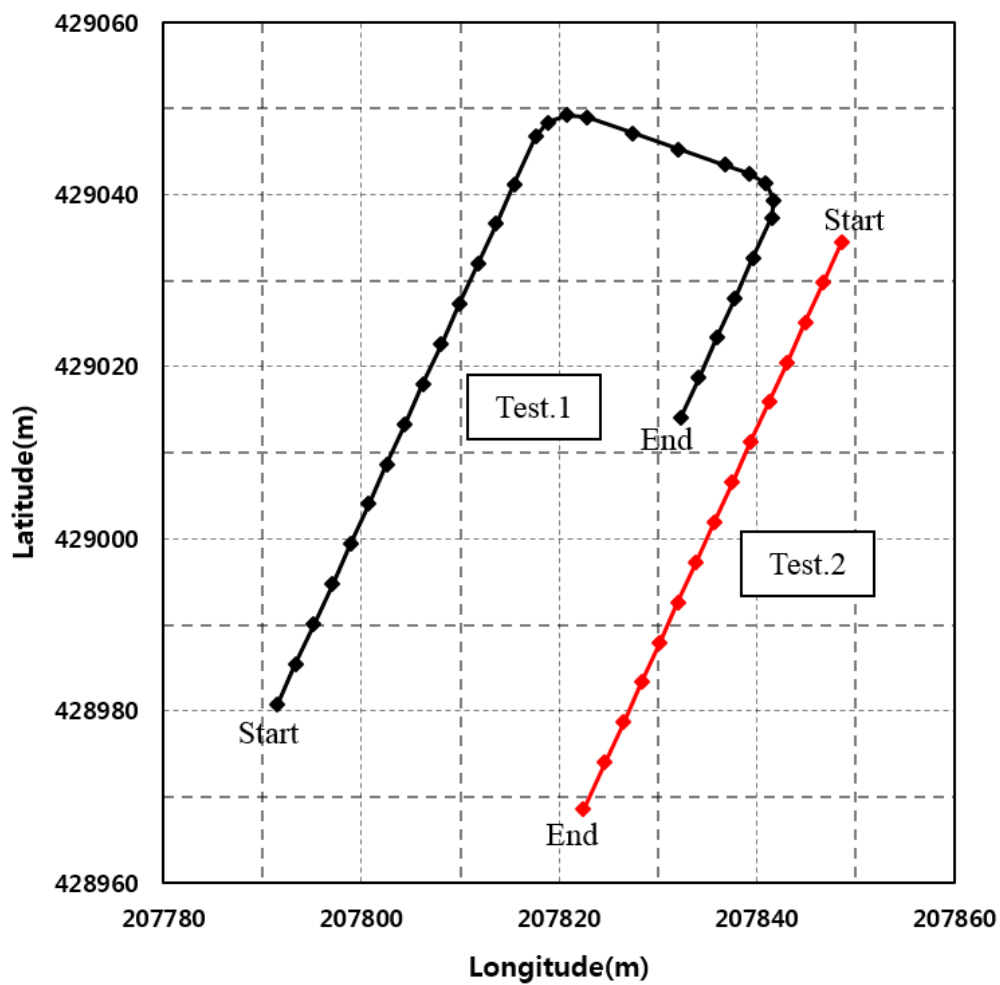
**Fig. 53 Overhead view of experiment trajectory.**

**Fig. 54 Photograph of path tracking test.**

## 2.6.6.　　　Evaluation Method of Path Tracking Deviation

To easily calculate the tracking error, the absolute coordinates were converted into relative coordinates, and the straight and curved paths were calculated separately (Fig. 55).

Fig. 56 shows a graphical visualization of the tracking error concept. For a straight path, the tracking errors were obtained by calculating the vertical distance of the path from the tractor position coordinates, shown in Equation (22).

For a curved path, the distance between the center of the curvature and the tractor was calculated by subtracting the radius, shown in Equation (23). The RMS error was calculated using Equation (24).
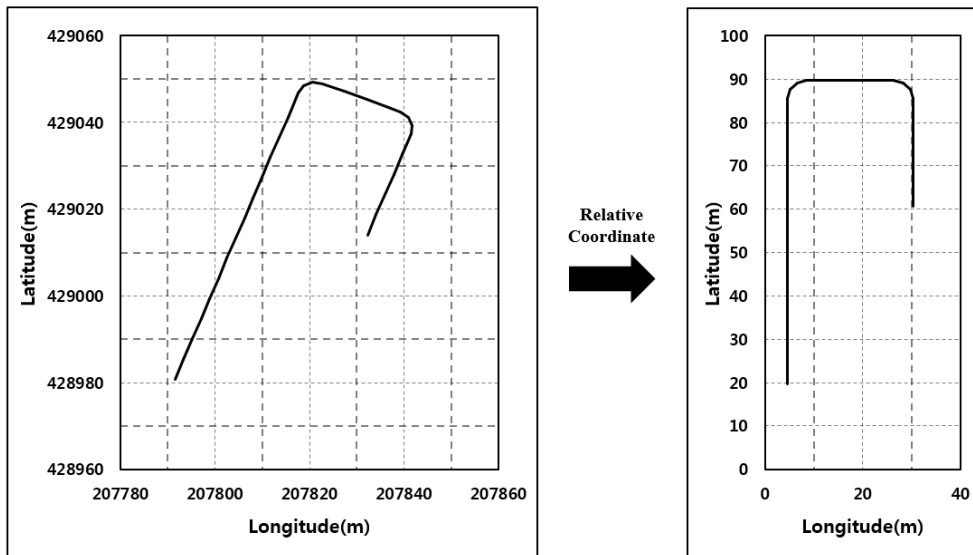


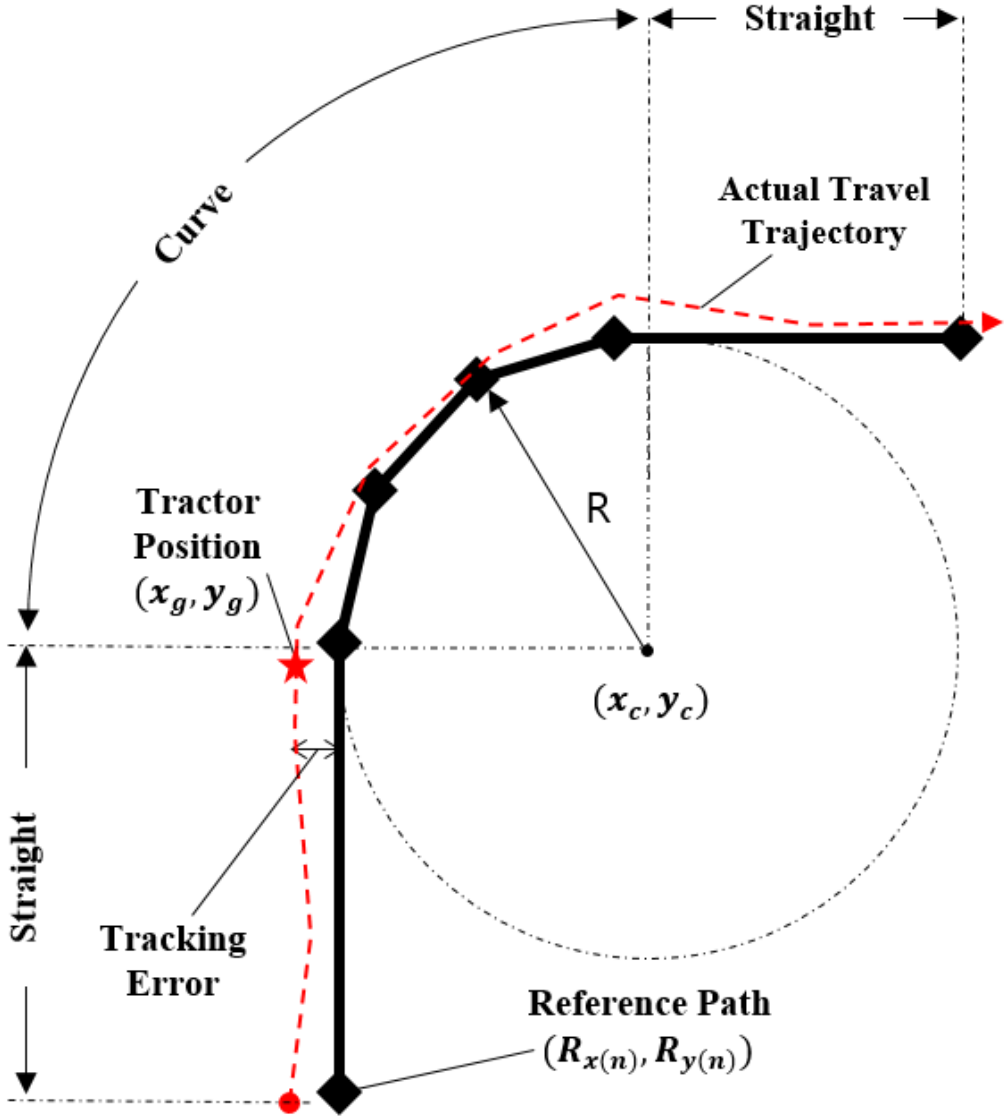**Fig. 55 Transformation of relative coordinates.**

**Fig. 56 Graphical visualization of the tracking error concept.**

$$\text{Tracking Error(Straight)} = \begin{cases} \left| x_g - R_{x(n)} \right| \\ \left| y_g - R_{y(n)} \right| \end{cases} \qquad (22)$$

$$\text{Tracking Error(Curve)} = \left| \sqrt{(x_g - x_c)^2 + (y_g - y_c)^2} - R \right| \quad (23)$$

$$\text{RMSE} = \sqrt{\frac{\sum(Tracking\ Error)^2}{Number\ of\ data}} \qquad (24)$$

# Chapter 3. Results and Discussion

## 3.1. Preliminary Test Results of EPS-based Hydrostatic Steering System

Fig. 57 shows a graph of the response characteristics of the EPS-based steering system according to the step input command during a no-load state. The step input applied to the EPS resulted in a steady-state error of 10%. It took about 0.2 s for the EPS to respond and discharge the fluid through the hydrostatic valve, and 0.42 s for the push forces of the steering cylinder to exceed the static friction force. The EPS-based steering system showed a slow response with a dead time of 0.42 s. When traveling at a speed of 2 km/h, this may ideally cause an error of about 7.4 cm, and if the speed is accelerated, the error may increase.
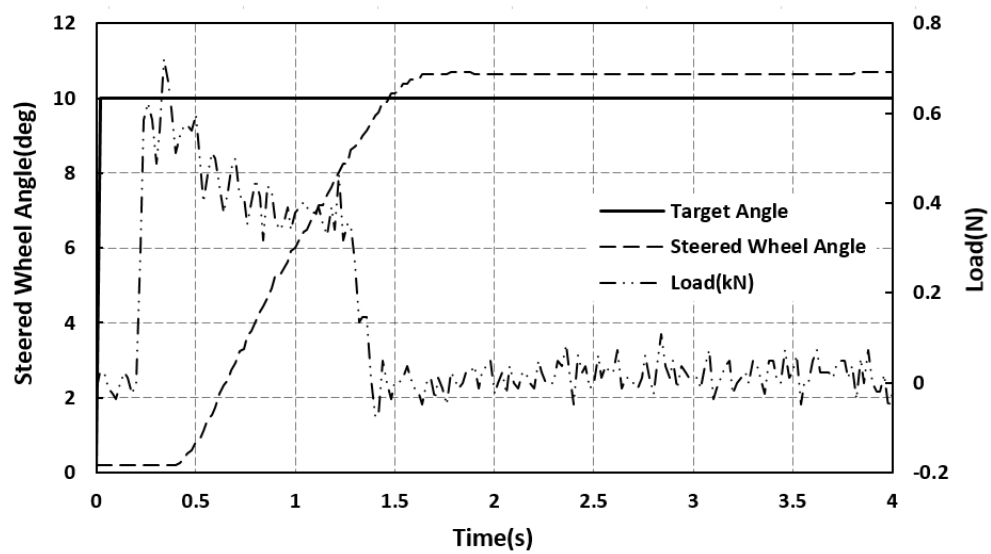
**Fig. 57 10° step response and load variation of vehicle with EPS-based steering system.**

Fig. 58 shows the load data of the steering cylinder according to the driving states of the tractor. A load of about 656N was generated under no-load conditions, and at a traveling speed of 3, 1, and 0, a load of 1165, 1548, and 9380N occurred, respectively. As the traveling speed was decreased, the magnitude of the load tended to decrease. The load data obtained from this experiment were reflected in the load system design of the HIL simulator, and the magnitude of the load to be used in the experiments was determined.
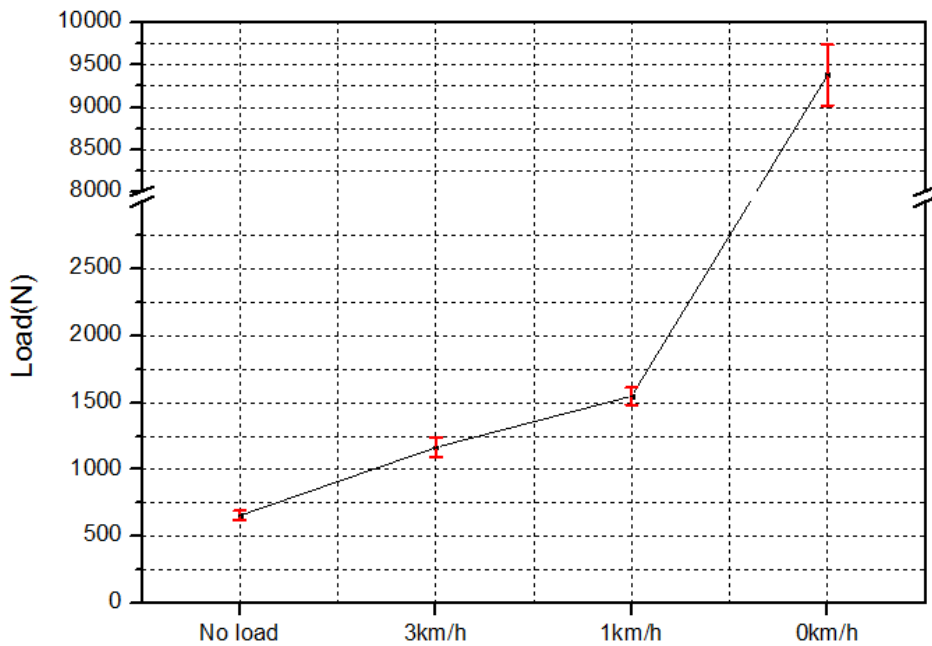


**Fig. 58 Load magnitude according to the traveling speed.**

## 3.2. Experiment Results of Steering Behavior of Hydrostatic Steering System using HIL simulator

The steering cylinder displacements depend on the integrated steering system and its turning capability. Fig. 59 shows the results of cylinder displacement based on the steering wheel angle as a comparison. The steering cylinder did not operate at a steering wheel angle of up to $\pm 10°$, and the displacement was kept constant with respect to the rotation. A large dead band ($\pm 10°$) was caused by the overlapping design of the hydrostatic valve and the static friction of the steering cylinder.

**Fig. 59 Relationship between the steering wheel angle and cylinder displacement.**

Fig. 60 shows results of the pressure and displacement of the steering cylinder based on the steering wheel angle. The pressures inside the steering cylinder remained constant until the steering wheel was rotated +5°. When the angle exceeded +5°, both chamber pressures began to change, which means that hydraulic fluid began to be supplied to the cylinder from the hydrostatic valve. When the steering wheel angle exceeded 10°, the displacement began to change.

The above results show that the hydrostatic valve had an overlap of ±5°, and a rotation of ±10° or more was required until the push force exceeded the maximum static friction of the steering cylinder.

The EPS-based steering system included a dead band of ±10°, which created a non-linear dynamic behavior in which it was difficult to drive exactly straight ahead at a relatively high traveling speed.

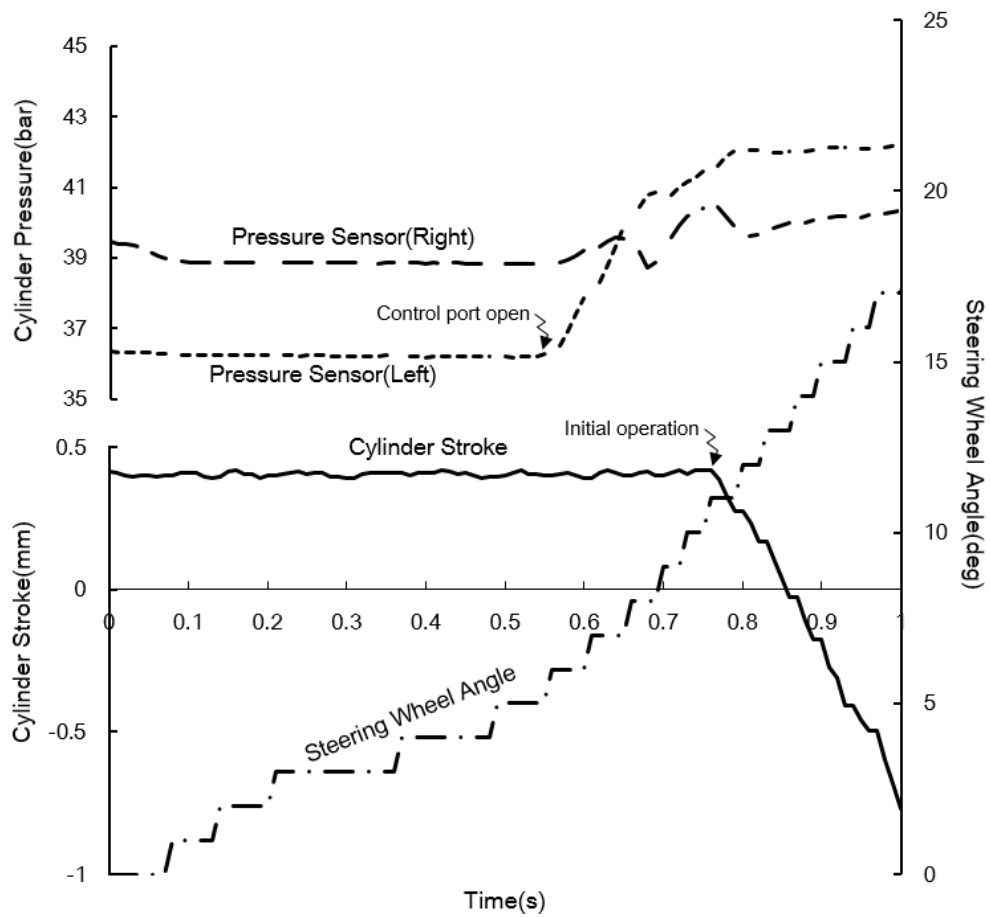**Fig. 600 Results of pressure and displacement of the steering cylinder based on the steering wheel angle.**

### 3.3.   Experiment Results of Electrohydraulic Steering System using HIL simulator

#### 3.3.1.   Dead-Time Approximation

Fig. 61 shows the data before and after applying the dead-time compensator using the HIL simulator, and utilizing steering commands of -5° and +5° in a sine wave pattern at a frequency of 0.25 Hz. Before applying the compensator, i.e., a proportional only (P) controller, an RMS angle error of 1.57°, and a signal delay of about 0.5 s were shown. On the other hand, when the compensator was applied, the RMS angle error was 0.88°, and the delay to the target angle was decreased. As shown in Fig. 62, after applying the dead-time compensator, the setpoint was compensated in terms of the delay-error amount. However, at a target angle of $\pm$5°, the point at which the target angle slowed, the steered wheel angle stopped before reaching the target angle because the spool position reached the dead band region.
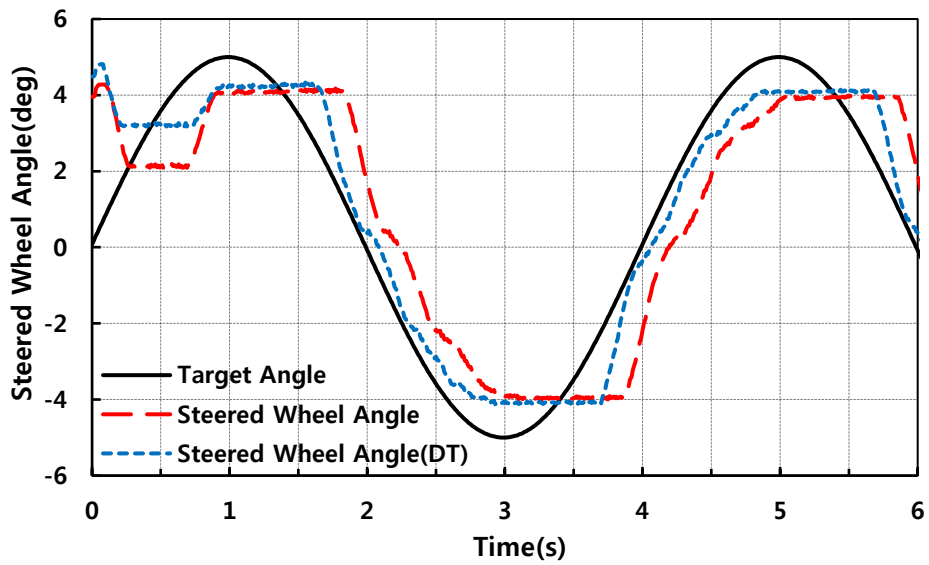
**Fig. 61 Sinusoidal test used for comparing the control algorithm with and without a dead-time compensator (DT).**
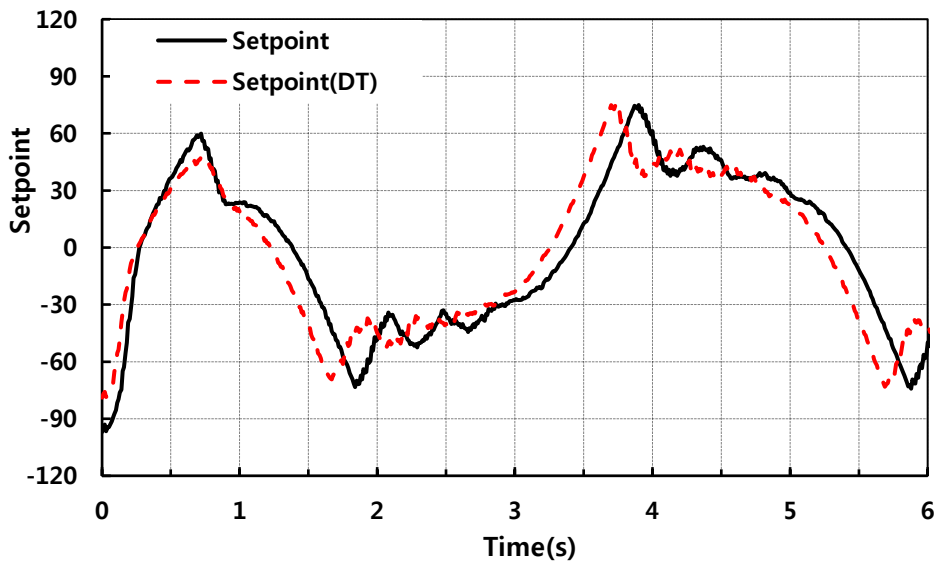


**Fig. 62 Control signal history with and without dead-time compensation (DT).**

### 3.3.2.    Dead-Band Compensation

Fig. 63 shows the data before and after applying the dead-band compensator using the HIL simulator, with steering commands of -5° and +5° in a sine wave pattern at a frequency of 0.25 Hz. Before applying the compensator, i.e., a proportional controller with a dead-time compensator, the RMS angle error was 0.88°, and the steered wheel angle stopped before reaching the target angle. On the other hand, when the compensator was applied, the RMS angle error was 0.61°, and the steered wheel angle nearly reached the target. As shown in Fig. 64, after applying the dead-band compensator, the dead band regions of the setpoint (-32 to +32) were removed. On the other hand, at the target angle of $\pm 5°$, when the direction of the velocity changed, the steered wheel angle started to move after a dead time of 0.35 s because static friction occurred when the direction of the velocity changed, which always incurs a a stopping state.
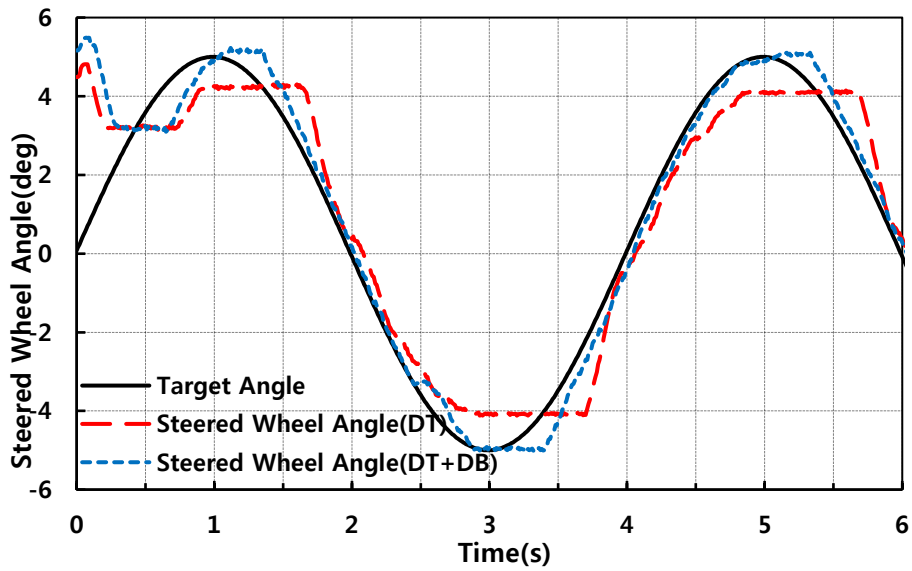
**Fig. 63 Sinusoidal test used for comparing the control algorithm with and without a dead-band compensator (DB).**
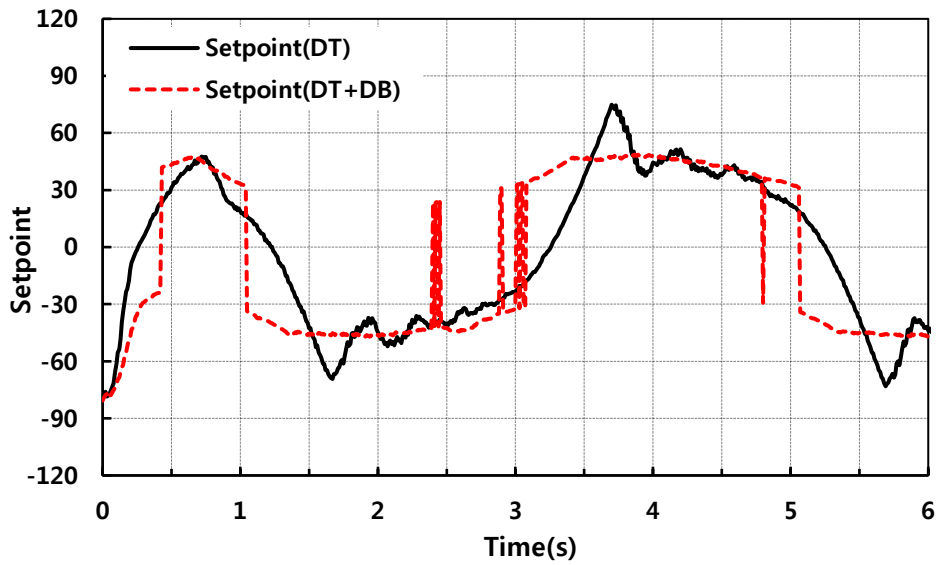


**Fig. 64 Control signal history with and without dead-band compensator (DT).**

### 3.3.3. Static Friction Compensation

Fig. 65 shows the data before and after applying the static friction compensator using the HIL simulator, where steering commands of -5° and +5°in a sine wave pattern at a frequency of 0.25 Hz were used. Before applying the compensator, i.e., a proportional controller with a dead-time and dead-band compensator, the RMS angle error was 0.61°, and the steered wheel angle started to move after a dead time of 0.35 s. On the other hand, when the compensator was applied, the RMS angle error was 0.50°. The steered wheel angle started to move after a stopping time of 0.2 s because of the use of the EHPV with an overlap, which caused a backlash in the closed-loop response.

As shown in Fig. 66, after applying the static friction compensator, an impulse signal was generated when the controller received a steering command for a directional change and exceeded the threshold values, which was converted instantaneously from static friction into kinetic friction.
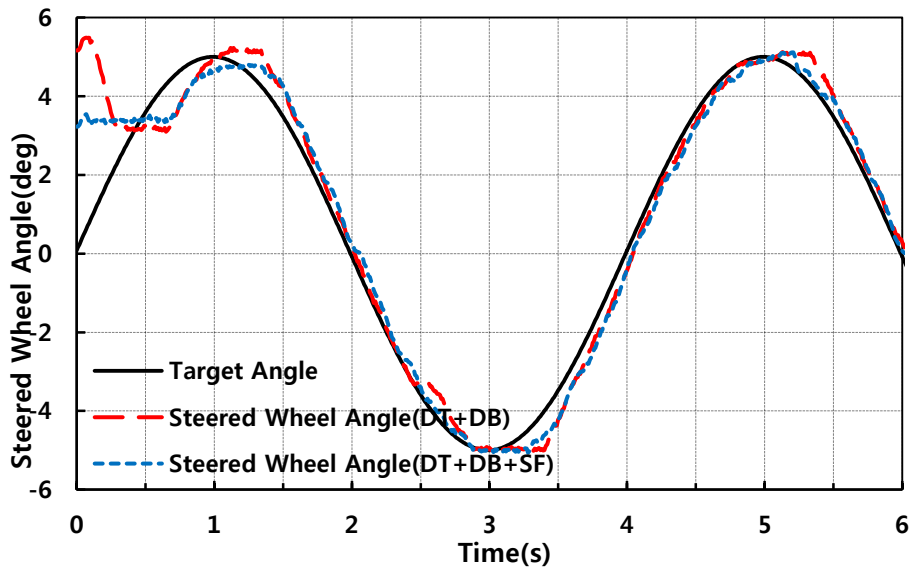
**Fig. 65 Sinusoidal test used for comparing the control algorithm with and without a static friction compensator (SF).**
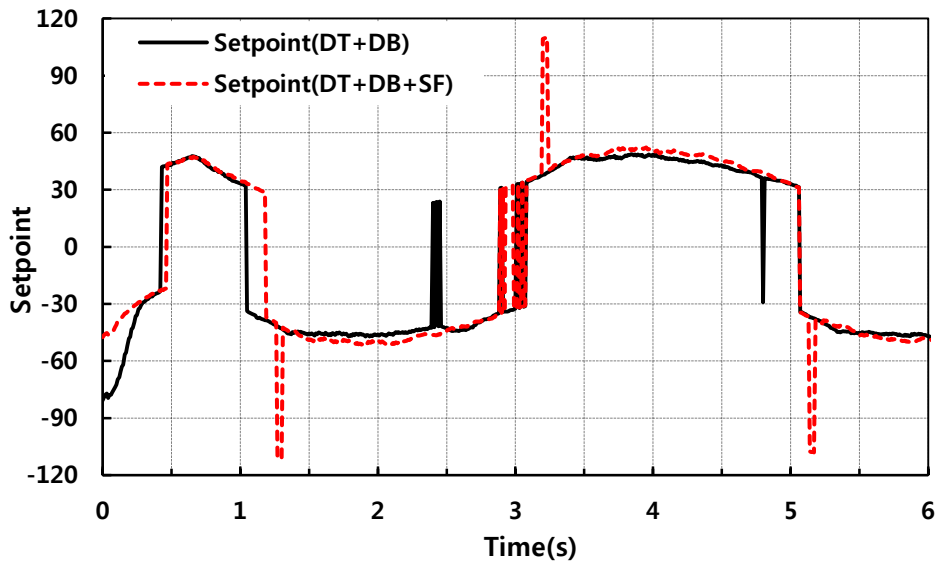


**Fig. 66 Control signal history with and without static friction compensator (SF).**

### 3.3.4.    Steering Controller Test under Load Conditions

Fig. 67 shows the performance of the steering controller under the load conditions using the HIL simulator when applying steering commands of -5° and +5° in a sine wave pattern at a frequency of 0.25 Hz. When loads of 0 to 1200 N were applied, the RMS angle error was 0.48, which indicates a good steering performance. However, when the loads were increased up to 2300 N, the RMS angle error reached 0.83. As shown in Fig. 58, the maximum loads were less than 1500 N during the actual traveling state, and thus the steering controller was judged to be suitable for tractor application.
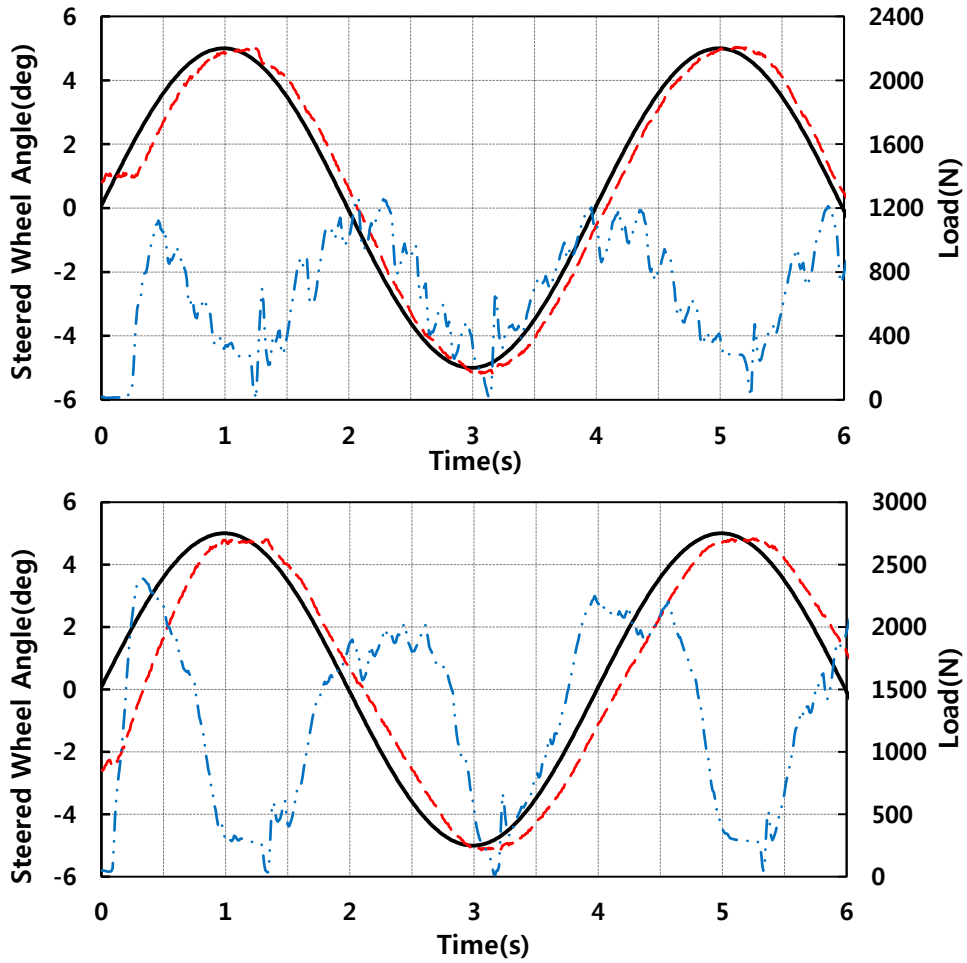
**Fig. 67 Results of the steering controller implemented on the HIL simulator under a steering command with a 0.25 Hz sinusoidal input and a loaded state. Operating load range of 0 – 1200 N (upper) and 0 – 2300 N (lower). The solid line indicates the target angle, the dashed line is the steering wheel angle, and the dashed-dotted line is the load.**

## 3.4.    Performance Evaluation of Tractor Steering System

### 3.4.1.    Zero Load Test

Fig. 68 shows a comparison of the response time based on the steering wheel angle between the EPS- and EHPV-based steering systems under no-load conditions. The EPS system took 1.5 s to reach the target, and the initial cylinder movement appeared at 0.4 s. On the other hand, the EHPV system took 0.7 s to reach the target, and initial cylinder movement appeared at 0.2 s. The application of the EHPV system improved the steering response by more than two-fold. To improve the performance of the EPS system, it was necessary to change to a high-torque motor because of the slow response times.
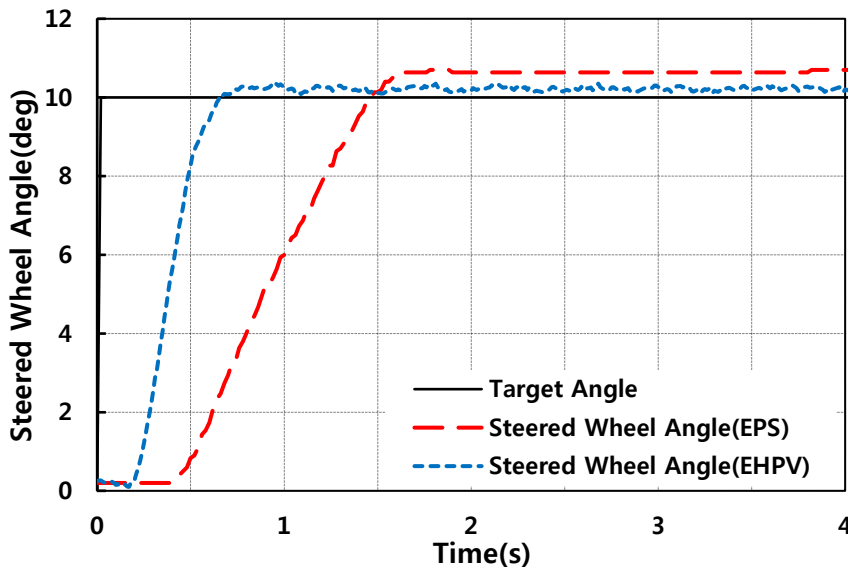


**Fig. 68 Comparison of experimental 10° step response times of the tractor when using the EPS- and EHPV-based steering systems under no-load conditions.**

### 3.4.2.　　　Sinusoidal Steering Test

Fig. 69 shows the results of the steering performance of the tractor at traveling speeds of 2 and 5.5 km/h, with steering commands of -5° and +5° in a sine wave pattern at a frequency of 0.25 Hz. The RMS angle error of the EPS system was 2.87° and 2.96° at a traveling speed of 2 and 5.5 km/h, respectively. The system was unable to follow the target angle quickly, and large errors in the angle occurred. On the other hand, the RMS angle error of the EHPV system was 0.62° and 0.86° at a traveling speed of 2 and 5.5 km/h, respectively. The EHPV system showed a faster steering response than the EPS system. However, the error increased owing to the change in the flow conditions.
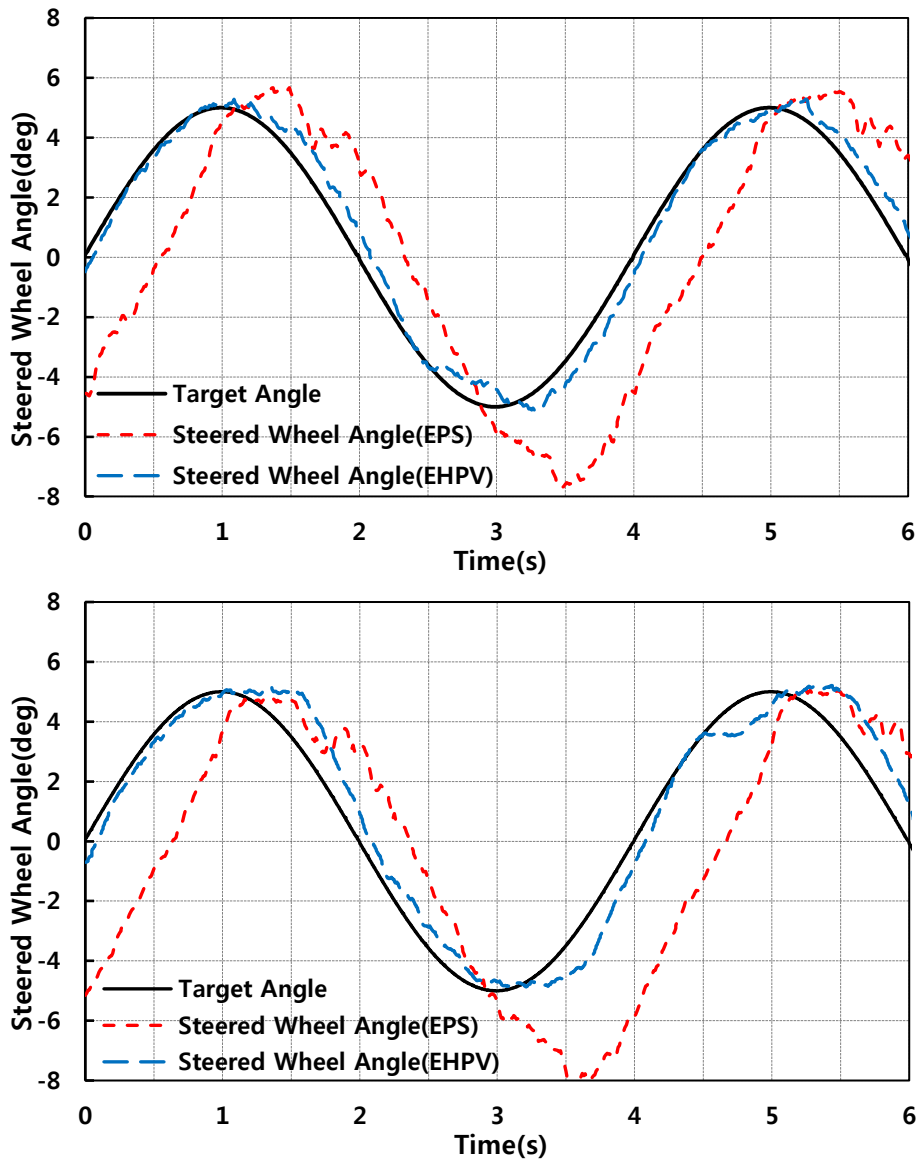
**Fig. 69 Comparison of sinusoidal test using the EPS- and EHPV-based steering systems. Traveling speeds of 2 km/h (upper) and 5.5 km/h (lower).**

### 3.4.3.    Path-Tracking Test

Fig. 70 shows the results of the auto-guidance tests for the Test 1 trajectory. The traveling speed of the tractor was 2 km/h. The experiment was performed using the TX803 test platform. The EPS system showed an RMS tracking error of 16 cm on the straight path and 26 cm on the curved path. On the other hand, the EHPV system showed an RMS tracking error of 12 cm on the straight path and 12 cm on the curved path (Fig. 72, left). On the straight path, there were no significant differences between the two systems, whereas on the curved path, a difference in RMS tracking error of 14 cm was observed. The adoption of the EHPV system resulted in a 29.3% improvement on the straight path, and a 50% improvement on the curved path.

For the full trajectory, the RMS angle error was 3.45° for the EPS system and 1.22° for the EHPV system (Figs. 71 and 72, right). The RMS angle error of the EHPV system was about 2.8-times lower than that of the EPS system.
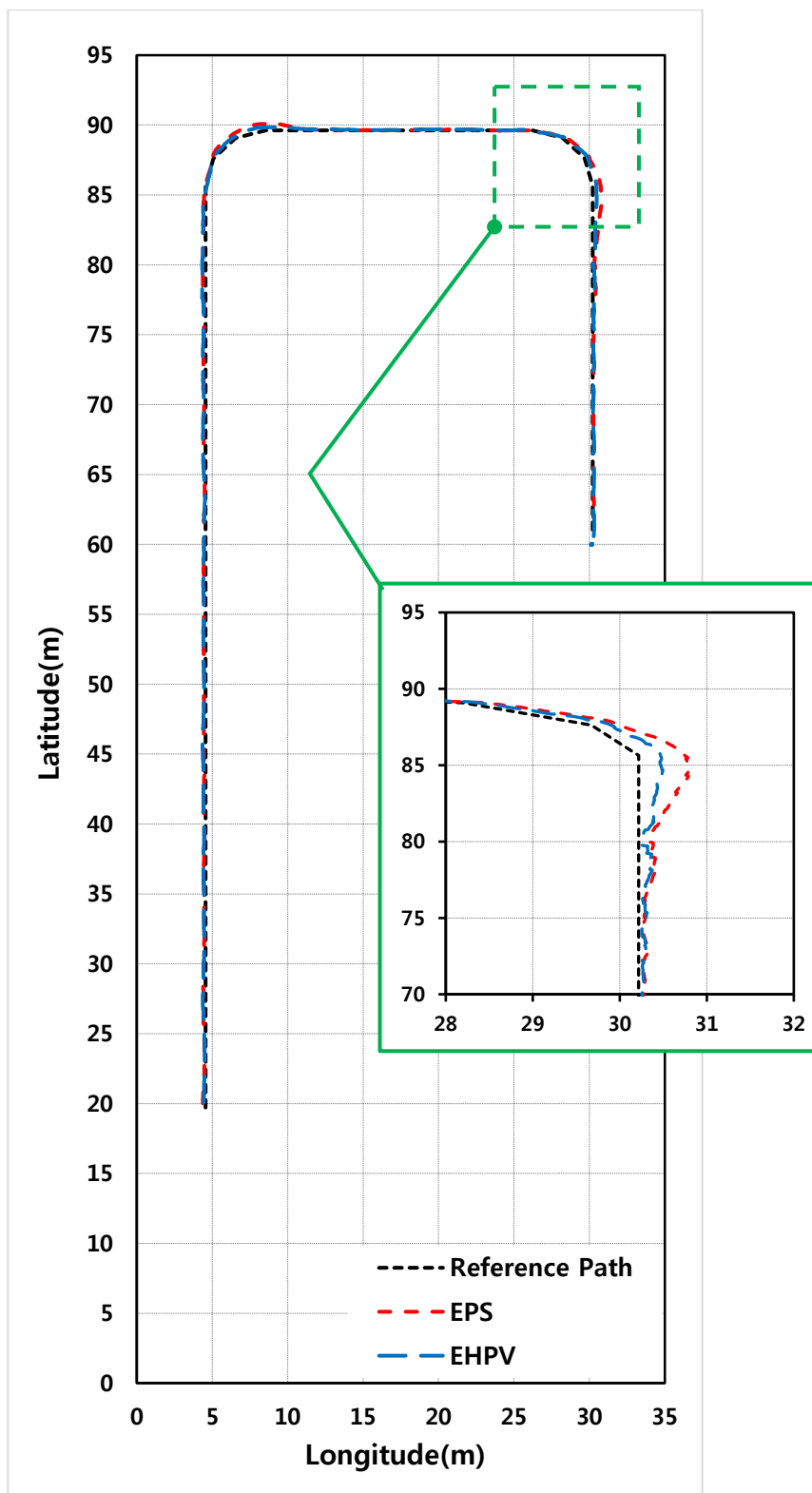
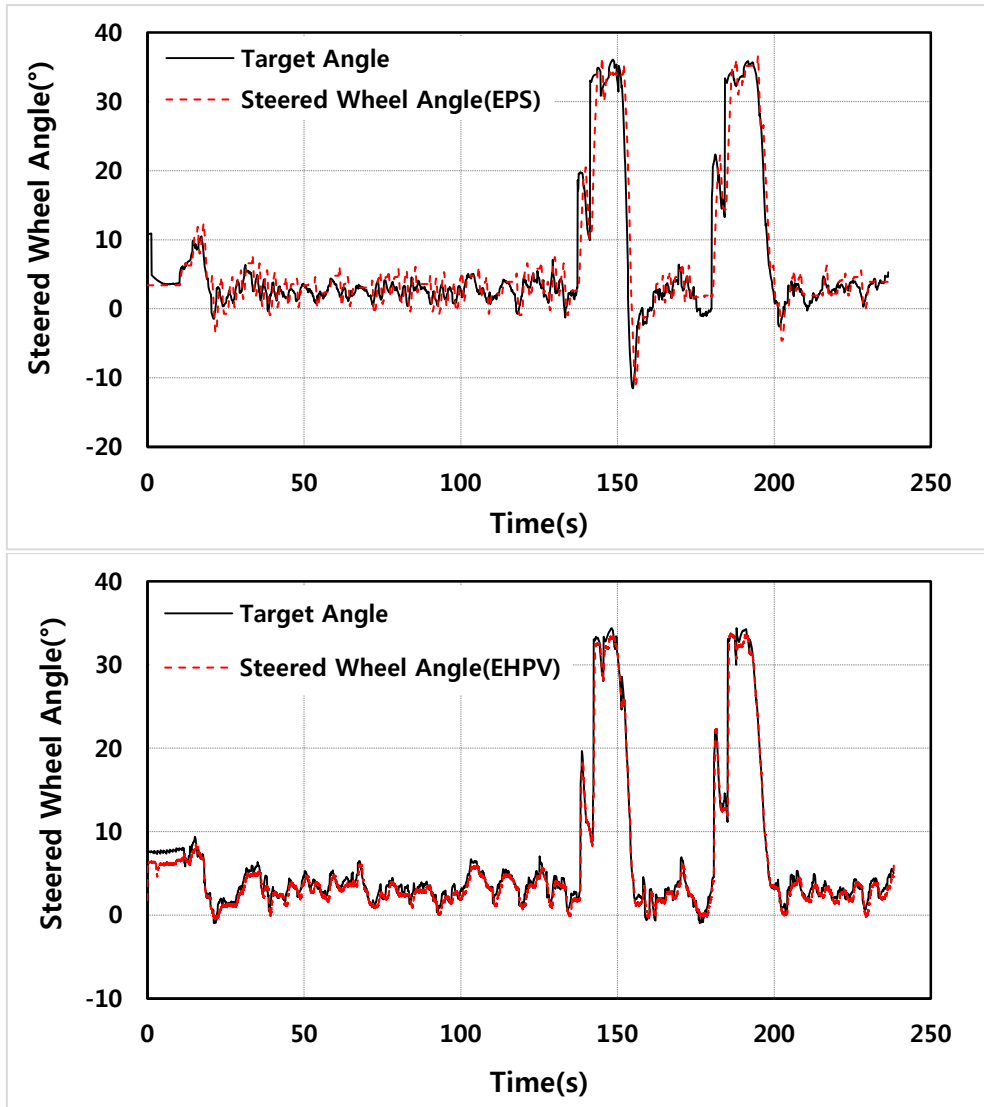**Fig. 70 Overhead view of experiment trajectory (Test 1).**

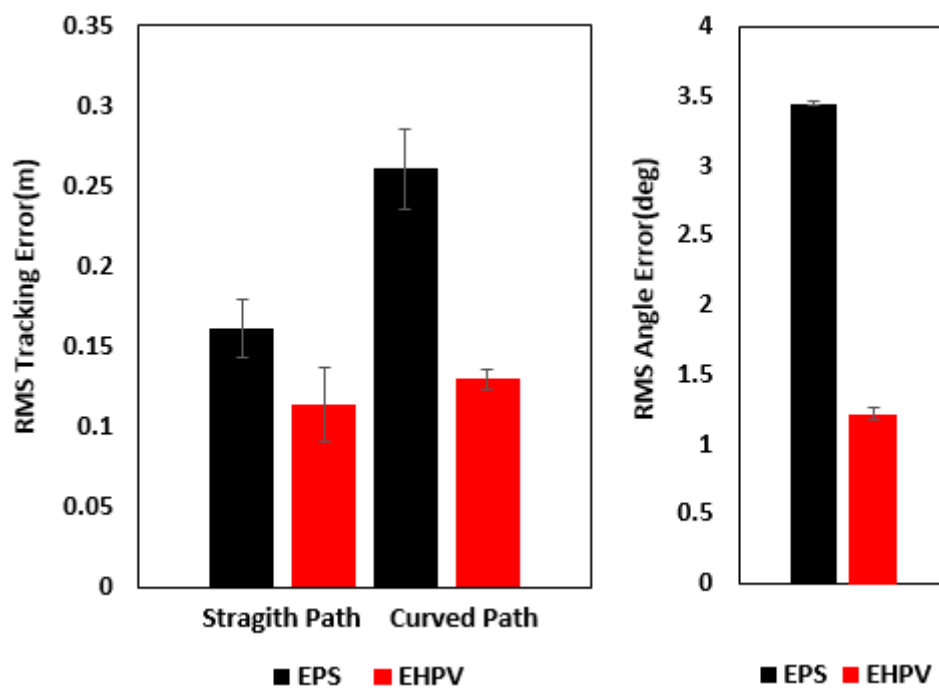**Fig. 71 Time history of steered wheel angle along the target angle.**

**Fig. 72 Bar graph showing the RMS tracking and angle errors for Test 1.**

Fig. 73 shows the results of auto-guidance tests for the Test 2 trajectory. The traveling speed of the tractor was 5.5 km/h. The EPS system showed an RMS tracking error of 20 cm on the straight path, and the tractor travelled in a sinusoidal wave-like pattern. On the other hand, the EHPV system showed an RMS tracking error of 12 cm on the straight path, with a relatively improved traveling pattern (Fig. 75, left). The RMS angle error was 11.3° for the EPS system, and 1.6° for the EHPV system (Figs. 74 and 75, right). The adoption of the EHPV system at a relatively high traveling speed resulted in an 85% improvement on the straight path. To improve the tracking performance of the EPS-based steering system at a relatively high traveling speed, the torque capacity of the motor must be changed, or an additional control algorithm that considers the delay characteristics of the actuator must be used.
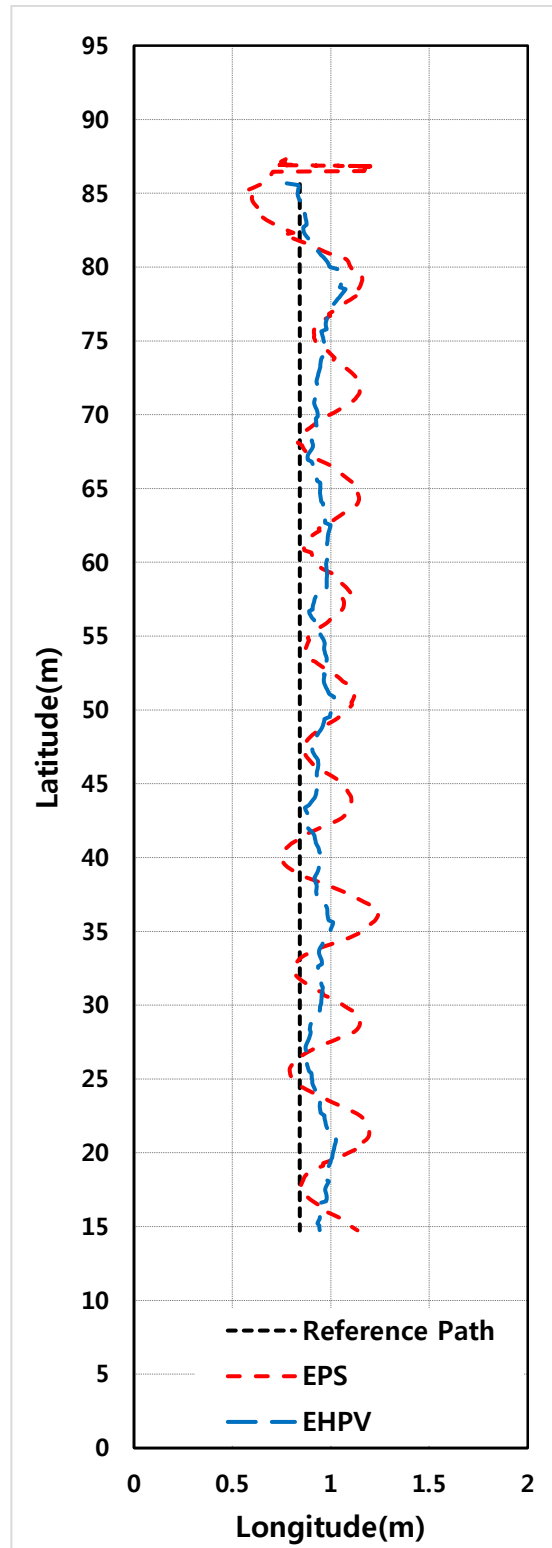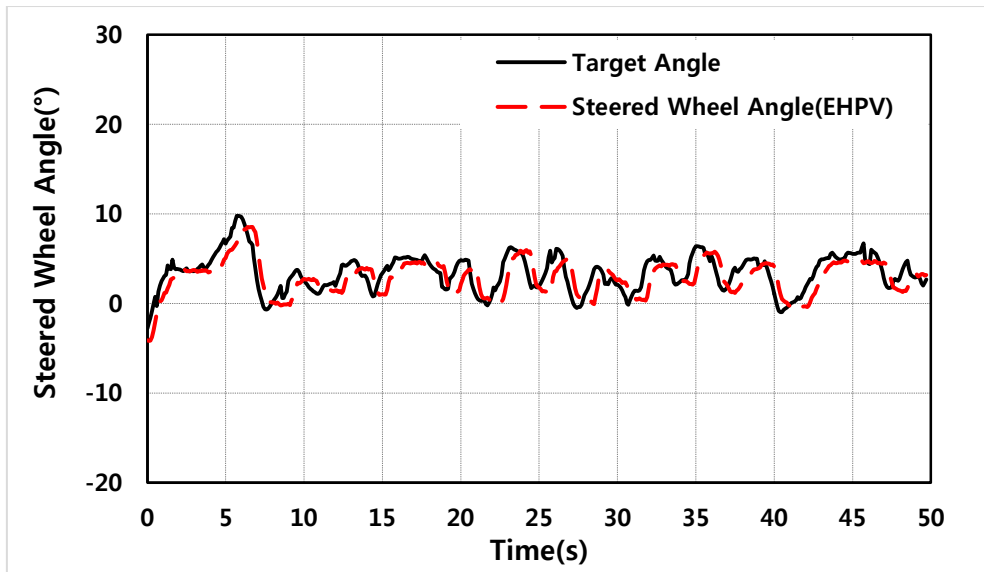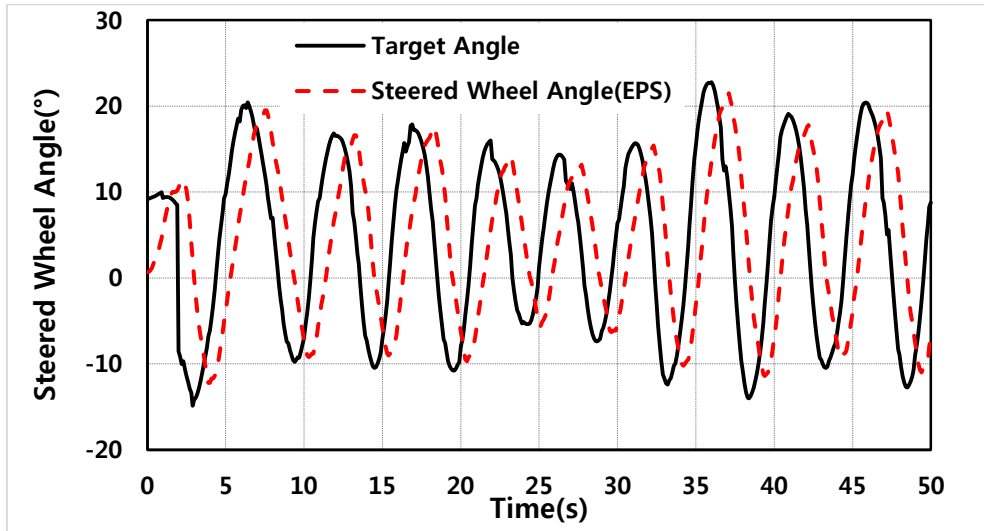
**Fig. 73 Overhead view of experiment trajectory (Test 2).**

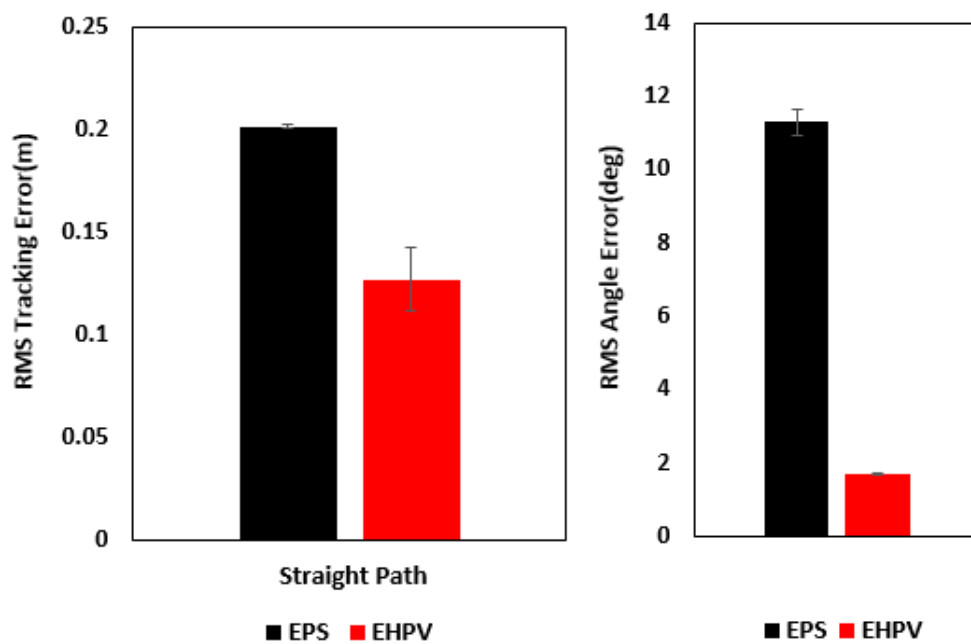**Fig. 74 Time history of steered wheel angle along with the target angle.**

**Fig. 75 Bar graph showing the RMS tracking and angle errors for Test 2.**

# Chapter 4. Conclusions

The main objective of this study was to develop an E/H vehicle steering system capable of auto-guidance, and to compare the performance of the developed system against a conventional automatic steering system. An E/H steering controller was developed based on linear feedback control combined with feedforward techniques, and was evaluated through sinusoidal response and trajectory tracking tests, the results of which were compared with those of the conventional steering system.

Several conclusions can be drawn from the results of this study:

1. An HIL steering simulator was developed for an analysis of the steering characteristics and control. The simulator provides an effective means for achieving a steering system design and steering controller.

2. Although a conventional hydrostatic valve showed an overlap of $\pm 5°$, a rotation of $\pm 10°$ was required to move the cylinder. The EPS-based steering system included a dead band of $\pm 10°$, which created a non-linear dynamic behavior.

3. A proportional-feedforward steering controller is a feasible solution to controlling and reducing any nonlinear characteristics.

4. An E/H steering controller was found to provide an adequate system performance at speeds of up to 5.5 km/h, and is considered to be a suitable steering system for high-speed operation such as during the spraying, seeding, tillage, and cutting processes.

5. A conventional steering system was shown to be suitable for a relatively lower speed. To improve the performance of the EPS-based steering system, the torque capacity of the motor must be changed, or an additional control algorithm that considers the delay characteristics of the actuator needs to be applied.

# Further Studies

The steering controller developed in this study showed an improved performance compared to a conventional steering system. However, it lacks the robustness necessary for a commercial-level application.

1. The weight variations of the tractor, such as the mounting devices or the farming workplace, will affect the steady-state performance of the steering system. It would be desirable to have a more robust controller for the steering valve. The performance of the actuator can be improved by incorporating the spool position or hydraulic fluid pressure feedback into the control scheme.

2. The dynamic viscosity of a liquid varies considerably with the temperature, and thus the hydraulic fluid used has a significant impact on the operation of a hydraulic system, specifically at low temperatures. Thus, a study on the effect of the steering performance based on changes in temperature is needed.

3. The dynamic performance of the tractor steering system was tested on a soil surface without conducting any farming operations. The effects of field operations on the steering dynamics should also be explored.

# 4. Bibliography

1. Amico, A. D. 2016. On electrohydraulic pressure control for power steering applications, PhD dissertation, Linkoping University

2. Deobelin, E. O. 1985. *Control system principles and design*, John Wiley & Sons

3. Diekhans, N. 2000. Electrohydraulic steering system. U. S. Patent No. 6,067,782

4. Ehsani. R., and E. Ontermaa. 2011. Application of auto-steering technology for tree planting, UF/IFAS Entension, University of Florida

5. Fischer, E., A. Sitte, J. Weber, E. Bergmann and M. Motte. 2016. Performance of an electro-hydraulic active steering system. *10$^{th}$ International Fluid Power Conference*, Dresden.

6. Han, X. Z. 2013. Development of path generation and tracking algorithms for an auto-guidance tillage tractor, MS thesis, Seoul National University

7. Han, X. Z. 2017. Development of path generation and robust tracking controller for unmanned tillage tractor in polygonal fields, PhD dissertation, Seoul National University

8. Harrer, M., and P. Pfeffer. 2015. *Steering handbook*, Springer

9. ISO, ISO. 11783-1: 2007. Tractors and machinery for agriculture and forestry--Serial control and communications data network--Part 1: General standard for mobile data communication

10. ISO, ISO. 11783-6: 2014. Tractors and machinery for agriculture and forestry--Serial control and communications data network--Part 6: Virtual terminal.

11. ISO, ISO. 11783-7: 2015. Tractors and machinery for agriculture and forestry--Serial control and communications data network--Part 7: Implement messages application layer

12. Jelali, M., and A. Kroll. 2002. *Hydraulic servo-systems.*

*Modeling, Identification and Control*, Springer

13. Jelali. M., and H. Schewarz. 1995. Nonlinear identification of hydraulic servo-drive systems, *IEEE Control Systems*

14. Jiang, M. M. 2009. Study on the position control of hydraulic cylinder for the E/H steering system in agriculture tractor, MS thesis, Kangwon National University

15. Leonard. N. E, and P. S. Krishnaprasad. 1992. Adaptive friction compensation for bi-directional low-velocity position tracking, Technical research report, University of Harvard

16. Mas, F. R., and Z. Qin, and A. C. H. 2010. *Mechatronics and intelligent systems for off-road vehicles*, Springer

17. Normey-Rico. J. E., and E. F. Camacho. 2007. *Control of dead-time process*, Springer

18. Nelson. F. W, and Waukee. 2006. Automatic steering system. U. S. Patent No. 7,349,779 B2

19. Qiu, H. C., Q. Zhang, J. Reid, and D. Wu. 1999. System identification of an electrohydraulic steering system. SAE Technical Paper, No 1999-01-2854.
https:// 10.4271/1999-01-2854.

20. Qiu. H. and Q. Zhang. 2003. Feedforward-plus-proportional-integral-derivative controller for an off-road vehicle electrohydraulic steering system. *Proceedings of the Institution of Mechanical Engineers Part D Journal of Automobile Engineering*.

21. Rekow. A. K. W., T. E. Schick, T. W. Rea, and R. J. Recker. 2007. Stable steering control system, U. S. Patent No. 0256884 A1

22. Stombaugh, T. 1997. Automatic guidance of agricultural vehicles at higher speeds. PhD dissertation, University of Illinois at Urbana-Champaign.

23. Winner, H., S. Hakuli, F. Lotz and C. Singer. 2015. *Handbook of driver assistance systems*, Springer

24. Ziaei. K. 1998. Development of a nonlinear adaptive control scheme for hydraulic actuators, MS thesis, University of Manitoba

25. Zhang, Q., J. F. Reid, and D. Wu. 2000. Hardware-in-the-loop simulator of an off-road vehicle electrohydraulic steering system. *Trans. ASAE*, 43(6), 1323-1330.

26. Zhang, Q. 2003. A generic fuzzy electrohydraulic steering controller for off-road vehicles. *Proceedings of the Institution of Mechanical Engineers, Part D: Journal of Automobile Engineering*, 217(9), 791-799

# 전자유압밸브를 이용한 자율 주행 트랙터 조향성능 향상 연구

## 이 창 주

## 국문 초록

 농업용 트랙터의 오토 스티어링을 위한 가장 대표적인 방법은 단순하고 저렴한 방법인 정유압 밸브 방식의 유압 스티어링 시스템에 전기 모터 시스템(EPS)을 결합한 형태이다. 그러나 정유압 밸브는 오버랩(overlap) 또는 불감대(dead band)가 설계되어 있다. 따라서 다양한 농작업에 사용되는 트랙터의 조향 성능이 제한적이며 잠재적인 이익을 극대화하는데 한계가 있다. 본 연구의 목적은 전자유압 조향 시스템 개발을 목표로 하며 기존의 정유압 조향 시스템과 성능을 비교하고자 하였다. 비례 – 피드 포워드 조향제어 알고리즘을 통해 트랙터의 유압 실린더의 비선형 특성을 효과적으로 보상하였다. 정유압 밸브와 비례제어밸브 두 가지 유형의 밸브로 구성된 컴퓨터 제어 HIL (Hardware-in-the-Loop) 조향 시뮬레이터는 조향제어 알고리즘을 개발하기 위해 설계 및 제작되었다. EHPV 및 EPS 조향 시스템이 장착된 RTK-GPS기반 자율주행 트랙터를 사용하여 자율주행 추종 성능을 필드 실험을 통해 비교 평가 하였다. 전자유압 조향 시스템은 기존의 시스템 보다 직선 경로에서 약 29%, 선회 경로에서 약 50%의 개선된 경로 오차가 나타났다.